HAC REF G2937

HIGH BRIGHTNESS DIODE LASERS FOR BLUE-GREEN APPLICATIONS

R.A. Mullen, D.J. Vickers, G.C. Valley, D.M. Pepper, and R.C. Lind

Hughes Research Laboratories
3011 Malibu Canyon Road
Malibu, California 90265

March 1990

N00014-87-C-0122
Final Report
December 31, 1988 through August 31, 1989

OFFICE OF NAVAL RESEARCH
800 N. Quincy Street
Arlington, VA 22217-5000

UNCLASSIFIED

SECURITY CLASSIFICATION OF THIS PAGE

REPORT DOCUMENTATION PAGE

Form Approved OMB No. 0704-0188

1a. REPORT SECURITY CLASSIFICATION: Unclassified

1b. RESTRICTIVE MARKINGS

2a. SECURITY CLASSIFICATION AUTHORITY

3. DISTRIBUTION / AVAILABILITY OF REPORT

2b. DECLASSIFICATION / DOWNGRADING SCHEDULE

4. PERFORMING ORGANIZATION REPORT NUMBER(S)

5. MONITORING ORGANIZATION REPORT NUMBER(S)

6a. NAME OF PERFORMING ORGANIZATION: Hughes Research Laboratories

6b. OFFICE SYMBOL *(If applicable)*

7a. NAME OF MONITORING ORGANIZATION

6c. ADDRESS *(City, State, and ZIP Code)*: 3011 Malibu Canyon Road, Malibu, CA 90245, (213) 317-5000

7b. ADDRESS *(City, State, and ZIP Code)*

8a. NAME OF FUNDING / SPONSORING ORGANIZATION: Office of Naval Research

8b. OFFICE SYMBOL *(If applicable)*: ONR

9. PROCUREMENT INSTRUMENT IDENTIFICATION NUMBER: N00014-87-C-0122

8c. ADDRESS *(City, State, and ZIP Code)*: 800 N. Quincy Street, Arlington, VA 22217-5000

10. SOURCE OF FUNDING NUMBERS

PROGRAM ELEMENT NO.	PROJECT NO.	TASK NO.	WORK UNIT ACCESSION NO.

11. TITLE *(Include Security Classification)*: HIGH-BRIGHTNESS DIODE LASERS FOR BLUE-GREEN APPLICATIONS (U)

12. PERSONAL AUTHOR(S): Mullen, R.A., Vickers, D.J., Valley, G.C., Pepper, D.M., and Lind, R.C.

13a. TYPE OF REPORT	13b. TIME COVERED	14. DATE OF REPORT *(Year, Month, Day)*	15. PAGE COUNT
Final	FROM 88/12/3 TO 89/8/31	1990 March 12	47

16. SUPPLEMENTARY NOTATION

17. COSATI CODES			18. SUBJECT TERMS *(Continue on reverse if necessary and identify by block number)*
FIELD	GROUP	SUB-GROUP	

19. ABSTRACT *(Continue on reverse if necessary and identify by block number)*

The threshold for self-pumped optical phase conjugation via stimulated photorefractive scattering has been dramatically lowered by inserting a diffusely retroreflecting screen in the path of the beam exiting the crystal. Stable reflectivities of up to about 60% have been demonstrated in a crystal having too low a gain-length product to exhibit unseeded backward stimulated scattering. The phase-conjugate fidelity is also very good. This conjugator offers many practical advantages over previous photorefractive phase conjugators. The threshold of the device can be precisely controlled by adjusting the attenuation of the seed. The device operates both in the visible and at the infrared diode laser wavelengths. The conjugator's reflectivity and fidelity have been experimentally characterized as a function of the following parameters: pump and seed intensity, crystal angle with respect to the incident beam direction, crystal interaction length, crystal-lens separation, and aberration strength.

20. DISTRIBUTION / AVAILABILITY OF ABSTRACT
☐ UNCLASSIFIED / UNLIMITED ☒ SAME AS RPT. ☐ DTIC USERS

21. ABSTRACT SECURITY CLASSIFICATION: Unclassified

22a. NAME OF RESPONSIBLE INDIVIDUAL

22b. TELEPHONE *(Include Area Code)*

22c. OFFICE SYMBOL

DD Form 1473, JUN 86 *Previous editions are obsolete*

SECURITY CLASSIFICATION OF THIS PAGE

UNCLASSIFIED

TABLE OF CONTENTS

LIST OF ILLUSTRATIONS

SECTION 1

INTRODUCTION

1.1 RELEVANCE TO NAVY

The low weight, compactness, affordability and very high wall-plug efficiency of modern diode lasers make them an extremely attractive choice for many laser applications. For submarine laser communications, diode lasers can be designed to operate at 911 nm, then doubled to the 455 nm wavelength at which the absorption spectra of deep ocean water has a minima. Photorefractive phase-conjugators offer advantages both in the development of high-power infra-red laser sources using phase-conjugate master-oscillator power-amplifier (PC MOPA)[1] diode laser scaling, and in the implementation of coherent communications underwater at blue-green wavelengths with photorefractive retromodulator/conjugators[2].

In the PC MOPA application[1], the capability of photorefractive conjugators to coherently combine several independently heat-sunk diode laser amplifiers has already been demonstrated (Air Force Weapons Lab Contract Number F29601-87-C-0029), as shown in Figure 1, and the development of a 2X9 array is underway. By using doubled 911 nm diode lasers (Graded index separate confinement heterostructure - GRINSCH - lasers having InGaAs active regions and AlGaAs cladding) in such a system, a photorefractively coupled high-power source at 455 nm could be realized for submarine laser communications.

More recently, the seeded stimulated photorefractive phase (SPS) conjugator developed on this program has been used in a retromodulator/conjugator[3,4] configuration to demonstrate coherent underwater communications through ocean water[2] (supported by Hughes IR&D). In this demonstration, Figure 2, the photorefractive conjugator removes many of the dynamic spatial

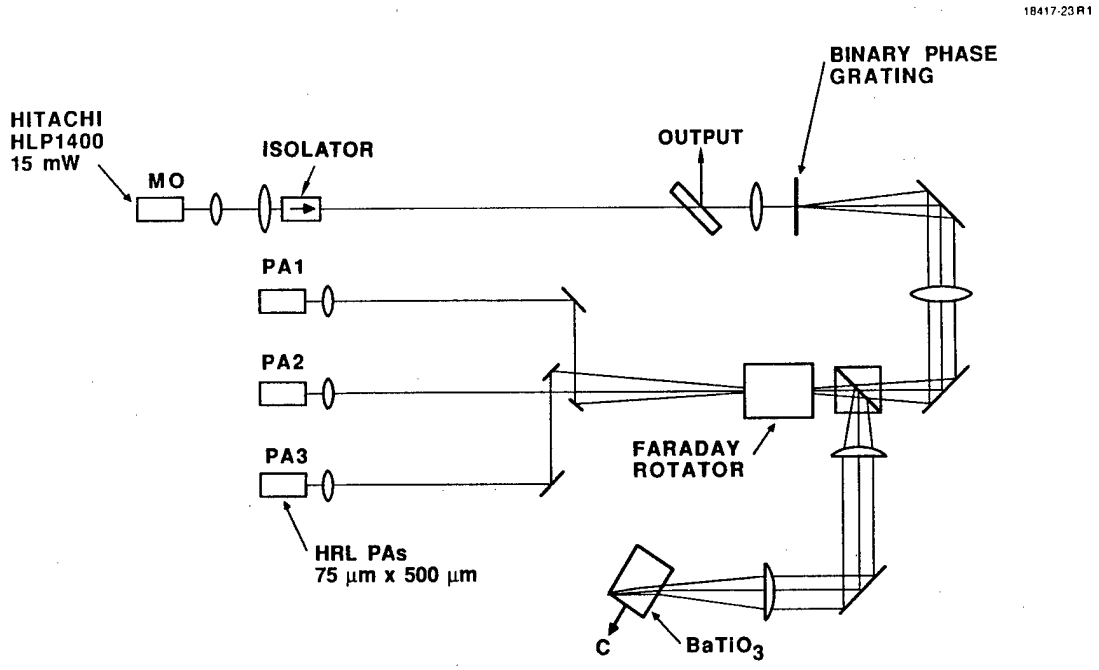

Figure 1. Diode PC MOPA. MO, master oscillator. PA, power amplifier. The binary phase grating splits the master oscillator output into three beams. In the amplifier chain, these beams experience double-pass amplification two times.

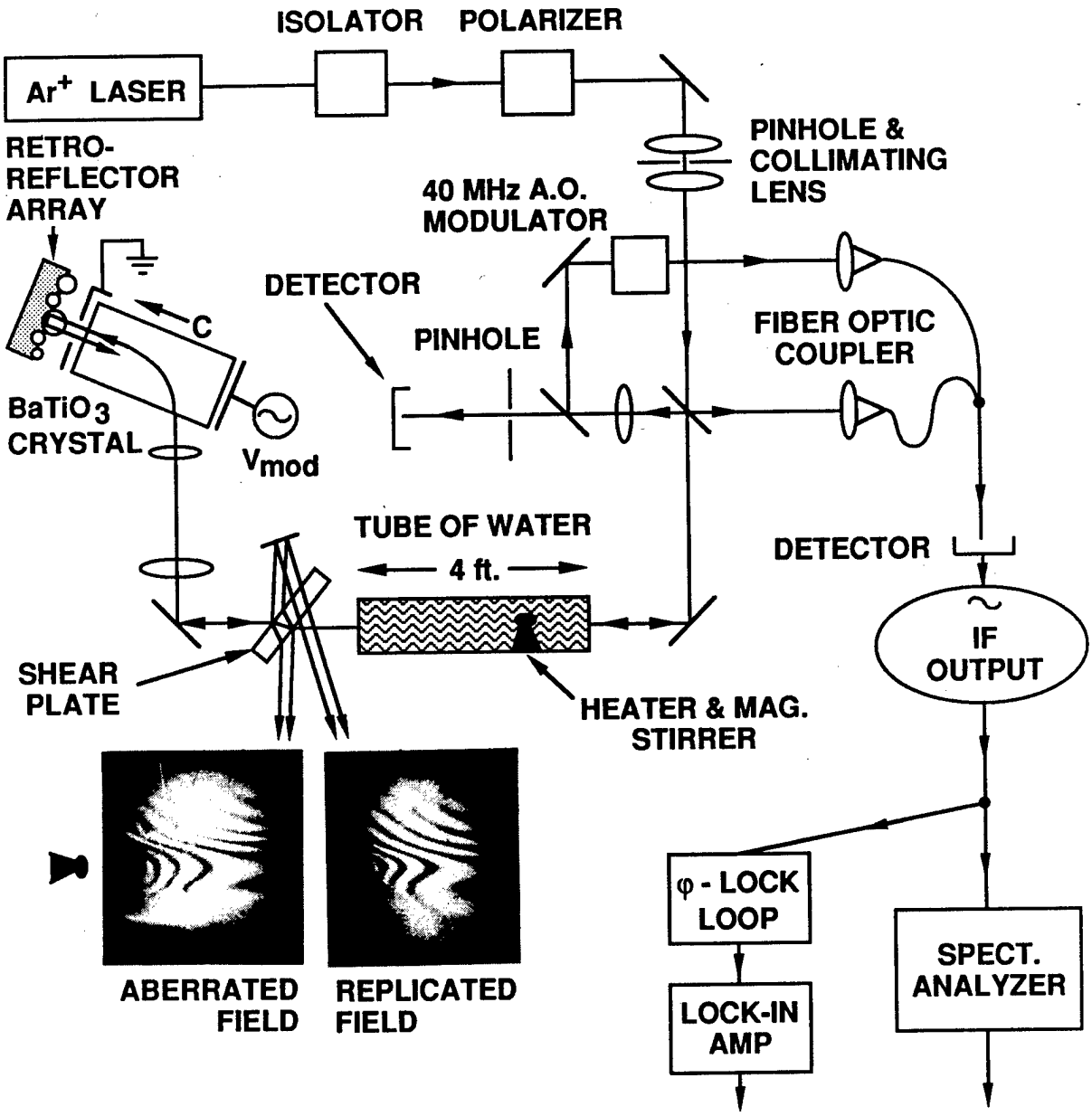

Figure 2. Underwater retromodulator/conjugator.

aberrations associated both with turbulence and dynamic scattering in water, making high bandwidth (GHz) coherent underwater communications realizable for the first time.

Another potential underwater application of photorefractive conjugators is in using them to build an optical gyroscope with multi-mode fibers. In this application, the photorefractive conjugator is used to compensate for the effects of modal dispersion and polarization scrambling which occurs in multi-mode fibers. This is important for gyro applications in order to assure that the various spatial modes retain the correct phase information as they propagate around the loops[5].

1.2 THE PROBLEM: TO DEMONSTRATE A SUITABLE PHASE CONJUGATOR

While many early feasibility demonstrations of the potential devices described above were performed with the standard "cat-conjugator," or internal loop geometry[6], this early geometry has several problems associated with it. Many of these problems arise from its reliance on the internal loop generated by total internal reflection of the fanned laser beam inside the crystal. This loop has been described as responsible for the formation of two discrete nonlinear interaction regions for phase conjugation via self-pumped four-wave mixing[7]. By contrast, the phase-conjugate device developed on this program has a single and much larger, extended interaction region, no internal loops, and no internal reflections[8-12].

Since the coherent coupling of multiple beams requires that all beams accurately overlap in the non-linear interaction region, the seeded SPS conjugator developed on this program offers an important practical advantage. Sufficient overlap between three beams in the earlier geometry involving the internal loop and dual-interaction regions geometry has been difficult to implement because of the problem of getting three separate beams to accurately overlap in these two small

interaction regions. Scaling to tens or hundreds of beams would be greatly facilitated by the availability of a conjugator having a single, larger interaction region. The seeded SPS conjugator developed on this program has this very important characteristic for diode laser scaling applications.

Speed of response is another potentially large advantage of the conjugator developed on this program. For applications to coherent underwater communications, the conjugator's speed of response is especially important. In this application, the photorefractive gratings inside the conjugator must be able to respond to dynamic variations in the laser's optical path (such changes can be induced both by relatively steady, slowly varying ocean currents as well as by faster small-scale turbulence effects). To the extent that existing models for the internal-loop conjugator are correct, a slower response time for the two-interaction region conjugator is to be expected, as a result of the importance of the large period gratings. By contrast, the gratings of importance in the seeded SPS conjugator are clearly the small-period gratings, known to have response times 10 to 50 times faster than the large period gratings[13].

The damage threshold of the seeded SPS conjugator is expected to be higher than that of the internal-loop conjugator, for several reasons. In the internal-loop conjugator, intense filaments of light circulate around inside the crystal and reflect from the inside surfaces of the crystal. This reduces the device's damage threshold in two ways. First, since surface damage thresholds are typically much lower than bulk damage thresholds, the internal-loop geometry will tend to exhibit lower damage thresholds than geometries not involving internal loops. Secondly, to the extent that the light circulates around inside this loop, passing through the small interaction regions multiple times, the intensity inside this loop (and particularly in the two interaction regions) will be higher than in a geometry requiring only single-pass traversal of the interaction region.

In the seeded SPS conjugator, there are no internal loops or internal reflections. High phase-conjugate fidelity builds up in the bulk of the crystal so that by the time the beam forms up into an intense filament, it is strongly depleted and is therefore less likely to cause surface damage when it reaches a crystal face than in the internal loop geometry.

Since there is only one interaction region involved in the externally seeded SPS conjugator developed on this program, and since there is clearly only one dominant grating (that arising from the interference of counterpropagating beams), the externally seeded SPS conjugator is much less complicated than the internal loop conjugator. Also, the similarity of the externally-seeded SPS to seeded stimulated Brillouin scattering (SBS) enables investigators to draw on the extensive SBS literature both for understanding the physics of the process as well for the transfer of SBS device demonstrations over to the SPS arena.

Prior to the work on this contract, there were only two reported observations of SPS in the literature. Chang and Hellwarth[14] made the first observation of SPS and recognized the close similarities between SPS and stimulated Brillouin scattering (SBS). With the crystal immersed in index-matching fluid, Chang and Hellwarth observed good phase-conjugate fidelity but relatively low reflectivities of ~10%. The published photo of the beam path inside the crystal immersed in the tank of index-matching fluid showed that the beam exiting the crystal struck the glass wall of the cuvette at nearly normal incidence. The authors correctly speculated that such "deliberate" scattering from the wall of the cuvette may have lowered the threshold for SPS. The Fresnel reflection from the cuvette wall may have seeded the SPS in this case, thus lowering the threshold for the process.

Without index-matching fluid, the SPS reflectivity in Chang and Hellwarth's experiments was unstable as a result of competition between two beam paths inside the crystal. Both of these beam paths were directed toward the corner of the crystal, and one of them resembled the loops typical of the conventional "cat conjugator," internal loop geometry[6].

Seeded backward gratings may also have played an important role in the observations of unstable and chaotic self-pumped phase-conjugation in $BaTiO_3$ crystals coated on both c-faces with perfectly diffuse white paint (European brand name Tipp-Ex, commonly known as Liquid Paper or White Out in the United States) in one experiment and with silver paint in another,[15] but the data and authors' interpretation of this work is not conclusive.

There have been two theoretical papers[16,17] on stimulated photorefractive scattering.

Mamaev and Shkunov[18] have recently demonstrated SPS phase conjugation in a thin $BaTiO_3$ butterfly-wing platelet of ~0.7 mm thickness. This material is grown by slow cooling of a $BaTiO_3$ + KF solution and differs from the larger top-seeded solution growth samples in that the butterfly wings have both a larger density of mobile charge centers (which result in increased gain per unit length) and a larger density of scattering defects. No external seed was required in this work, since the density of intrinsic defects was high enough to obtain above-threshold operation without an external seed.

For ordinary crystals having good optical quality, the gain-length product is less than the critical threshold value for SPS. The back-injected seed developed on this program enables one to obtain above threshold SPS in crystals which by themselves would either be too short or have too low a gain to operate above threshold. The seed lowers the threshold for SPS.

One final advantage of the externally seeded conjugator developed on this program (as compared to the internal loop conjugator) is that, since the seed is generated outside the crystal, the properties of the seed can be conveniently and

precisely controlled. As demonstrated by the data to be presented in Section 3, seeded SPS is a threshold process and the threshold can be precisely controlled by adjustment of the seed intensity. Thus, the conjugator can be modulated by switching the seed on and off. Moreover the system can be useful as a threshold detector. Finally, a common seed can in principle service an array of SPS conjugators, thereby phasing up the ensemble. The result is a large aperture conjugator. Other potential means for controlling the threshold include adjusting the phase of the seed, and adjusting the relative sizes of the seed-crystal separation relative to the laser coherence length.

SECTION 2

RETROREFLECTING SCREENS AS SEEDS FOR SPS

We found that the threshold for back-seeded stimulated photorefractive scattering (SPS) can be dramatically lowered by accurately redirecting a portion of the transmitted laser beam backwards into the photorefractive crystal. Using a retroreflective array as the seed, stable SPS reflectivities (without any internal reflections or circulating loops of light) of up to 60% were obtainable. The improved performance of the retroreflective array seeds over perfectly diffuse seeds is ascribed to the fact that the retroreflective seed closely redirects the transmitted light back onto itself. This results in greatly improved overlap of the seed with the forward-going filaments inside the crystal.

2.1 INITIAL EXPERIMENT

Our initial demonstration[9-11] of the very high effectiveness of using retroreflecting arrays as the seeds to lower the thresholds for backward SPS was done using the experimental apparatus shown in Figure 3. The 515 nm argon-ion laser beam was not spatial-filtered and contained a large number of high-order spatial modes.

Reflectivities of up to 60% were demonstrated in our initial observations of SPS seeded by retroreflective arrays. Top-view photographs of the beam trajectory as the SPS was building up are shown in Figure 4. In Figure 4a, there is no seed and no backward SPS. The beam refracts into an a-face of the crystal, fans[19] sharply towards the c-axis (by forward SPS[17,20]), and exits a c-face of the crystal as shown. In Figure 4b, a 3M #7615 retroreflector array is positioned to intercept the transmitted beam. The transmitted beam is thus injected directly backwards into the crystal, closely retracing the path of the forward-going

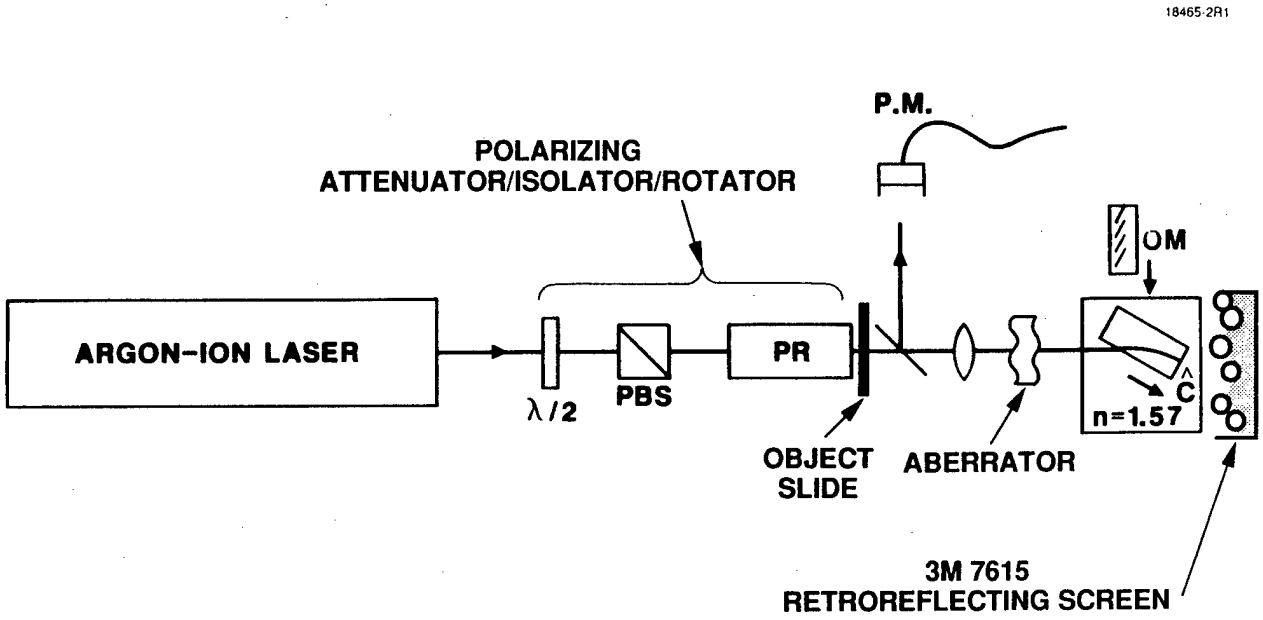

Figure 3. Initial experimental apparatus.

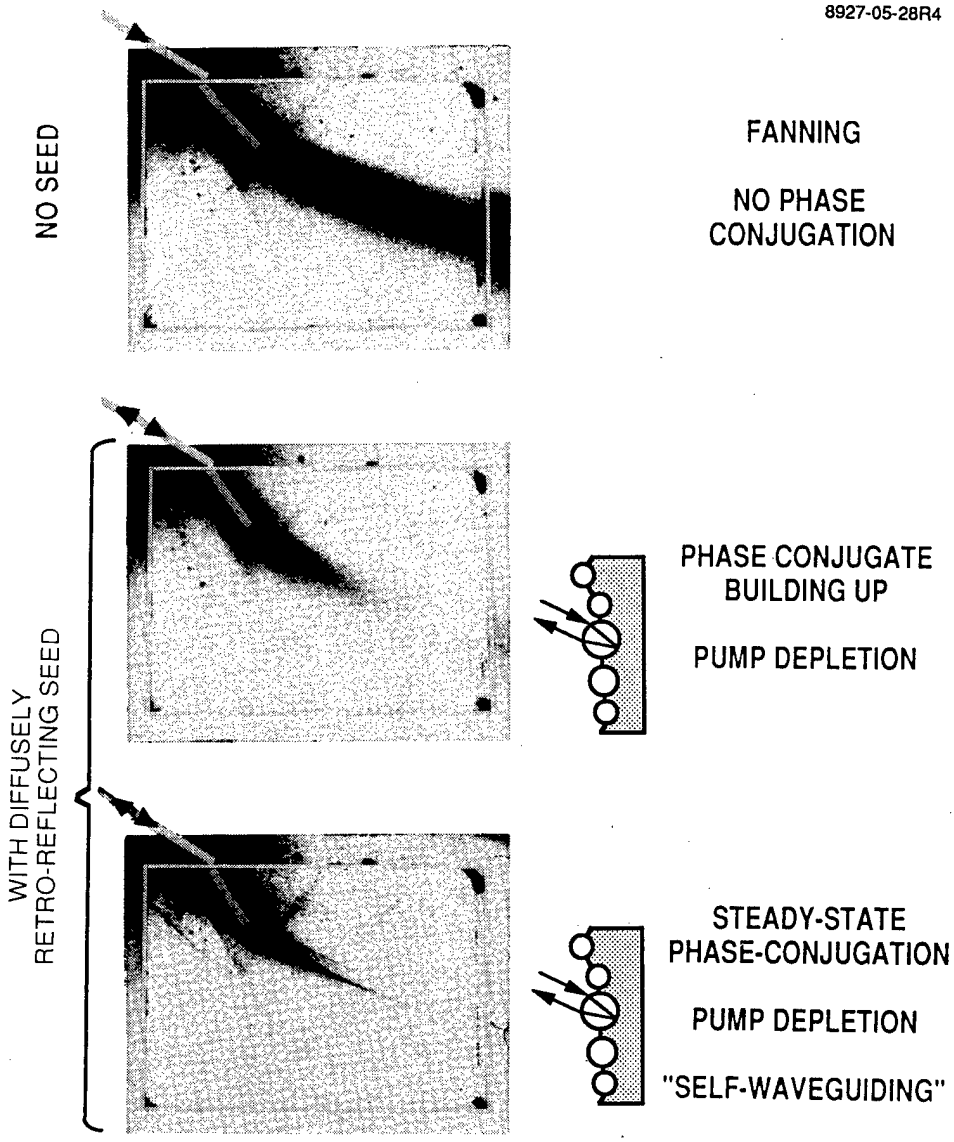

Figure 4. SPS Build-up sequence.

beam and dramatically lowering the gain for backward SPS. The phase-conjugate signal begins building up almost instantaneously (within a second). Figure 4b is a photo of the beam trajectory while the backward SPS is building up. Once the reflectivity builds up to its final steady-state value, the beam trajectory (Figure 4c) looks considerably different than in its transient state. The beam has formed into a relatively intense filament, as shown, indicating that some sort of "self-waveguiding" seems to be occurring.

The very high fidelity of seeded SPS phase conjugation is demonstrated by comparing the images of aberrated Air Force Resolution Charts after phase conjugation by the seeded SPS conjugator (Figure 5). In Figures 5(a) and 5(b) the 3M #7615 screen is used as the seed; the image in (a) has not been aberrated while the image in (b) has. The resolution in both these cases is comparable, about 5.7 line pairs per mm.

In (c), the crystal was removed from the index-matching fluid and its exit face was painted with "White Out," a nearly "perfectly" diffuse scatterer. Steady phase-conjugate reflectivities of about 8% were obtained by moving the crystal to a distance of 44 cm from the lens. At a 52 cm distance from the lens, the reflectivity was larger but unstable, having peak values of about 28%. We learned in later experiments, to be described in Section 3, that the index-matching fluid helped to stabilize the seeded conjugator. As such, a fairer comparison of the perfectly diffuse versus diffusely retroreflecting seeds was made by leaving the crystal in oil and replacing the retroreflecting screen with a screen painted with barium sulfate (another "perfectly" diffuse scatterer). In this case the reflectivity was stable but low (about 1%), and the fidelity was comparable to that seen with the retroreflecting screen as the seed.

The severity of the aberrator is evident from (d), in which the seeded SPS conjugator is replaced by an ordinary mirror.

8927-05-33R1

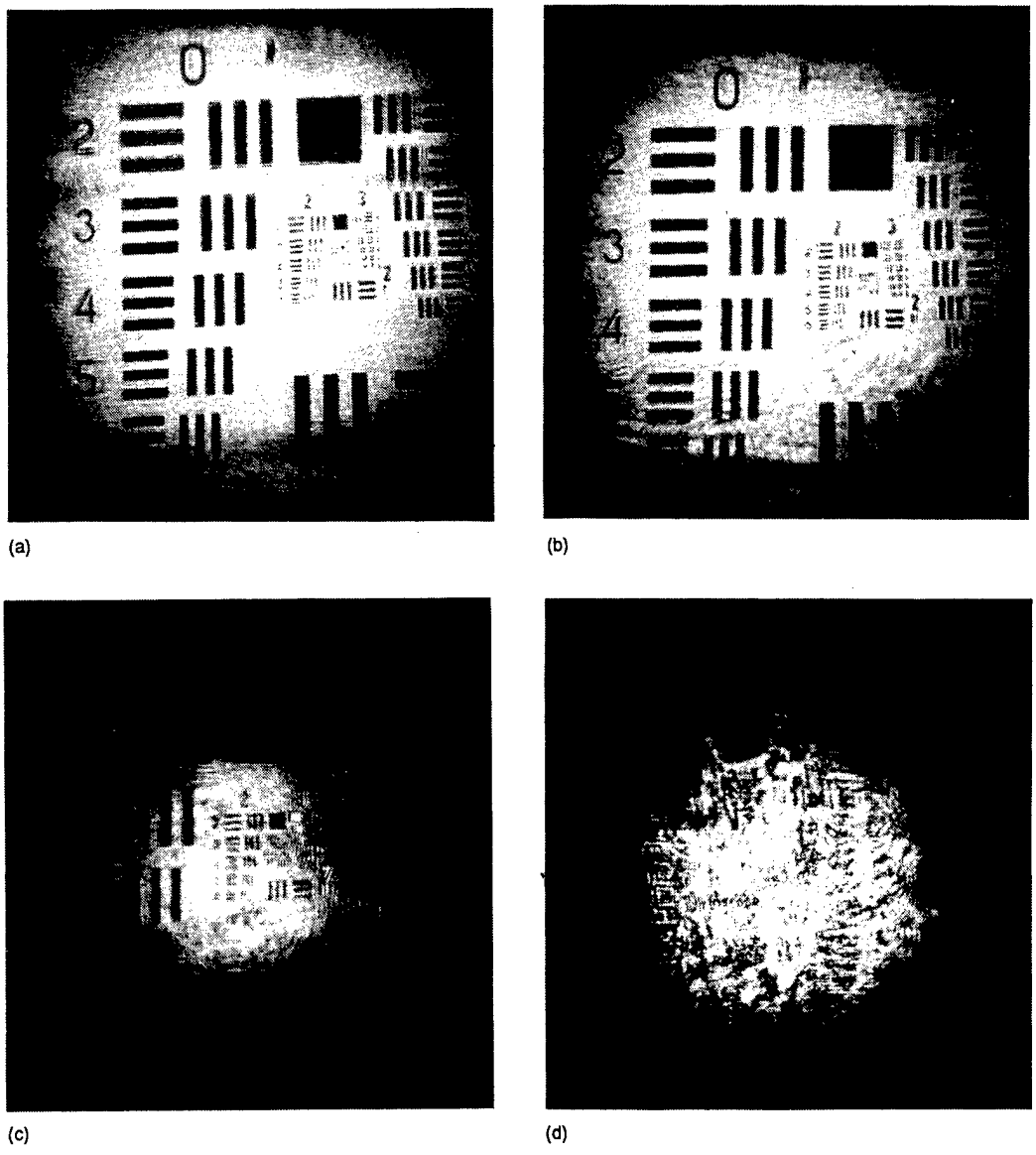

Figure 5. Images of Air Force Resolution Charts.

The highest phase-conjugate reflectivities were obtained by using a special effects projection screen #7615 as the retroreflecting seed. Detailed specifications of this screen are discussed in Section 2.2.

Operation at diode laser, helium-neon, and argon-ion laser wavelengths in geometries with and without index-matching fluid was obtained; details will be presented in Section 4.

Several alternative but considerably more complicated geometries for injecting phase-conjugate seeds to lower the threshold for SPS were described and experimentally characterized during the first half of this contract[20]. Retroreflective screens as seeds are much simpler to implement in practical applications than are phase-conjugate seeds.

2.2 RELEVANT PROPERTIES OF THE 3M #7615 RETROREFLECTOR ARRAY

The retroreflecting screens used as seeds in these experiments are described by their manufacturer, 3M Corporation, as a collection of half-silvered glass beads embedded in a plastic film. The beads are randomly arranged and vary in size, as shown in the photomicrograph in Figure 6, but the average bead diameter is about 40 μm. The beads which appear to be deformed in this picture probably scatter light over a somewhat wider angle than than would be associated with a perfectly retroreflecting screen. The angular divergence of the returned light, defined in Figure 7(a), is about 0.5°. Figure 7(b) is a plot of the retroreflective intensity as a function of observation angle θ relative to the angle of incidence displayed in Figure 7(b). The reflective intensity is strongly peaked directly backwards along the angle of incidence, dropping to e^{-1} at an observation angle of 0.5°. This means that for a crystal-to-retroreflector distance of 10 cm, the retroreflected light will re-enter the crystal within about 0.9 mm, an effective blurring which is surprisingly small compared to the laser spot size at the exit face of the crystal.

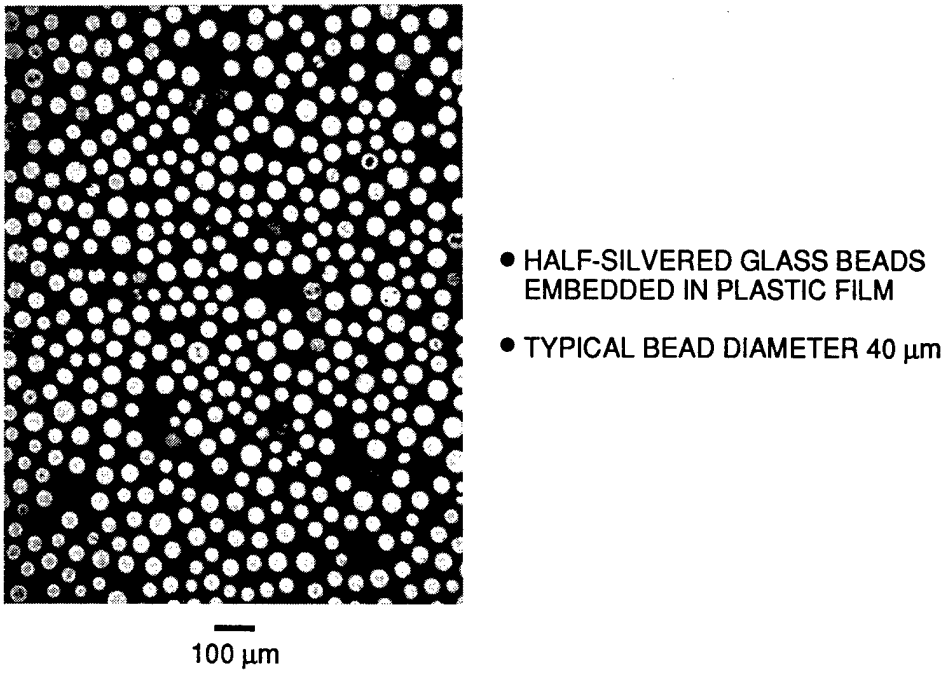

Figure 6. Photomicrograph of 3M #7615 special effects projection screen.

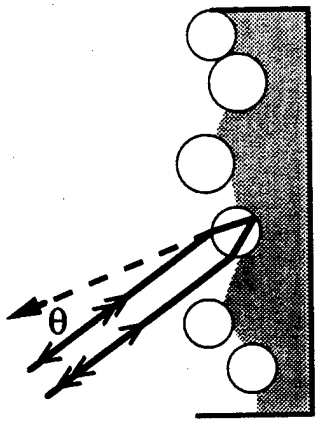

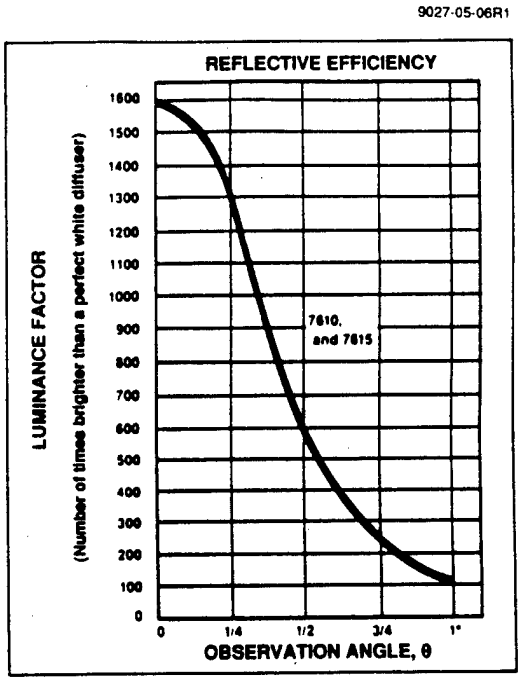

Figure 7. Retroreflecting accuracy of 3M Special Effects Projection Screen #7615.

The retroreflective efficiency of these screens remains high for angles of incidence as high as ±40° with respect to the angle of incidence, as shown in Figures 8(a) and 8(b). This is roughly the angle of incidence at which the retroreflecting efficiency drops to 1/e of its peak value. This means that there is a very wide tolerance on the orientational alignment of the retroreflector array relative to the incident beam direction, and that the retroreflective efficiency of the array is fairly uniform for incident beams having wide angular divergence.

Other retroreflective screens of interest for these applications include the reflexite brand name as well as other screens manufactured by 3M and other companies. The paint used in road signs is retroreflective as are many tapes used for children's clothing and athletic wear.

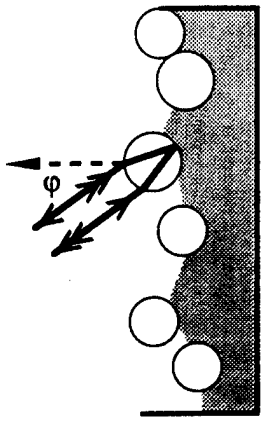

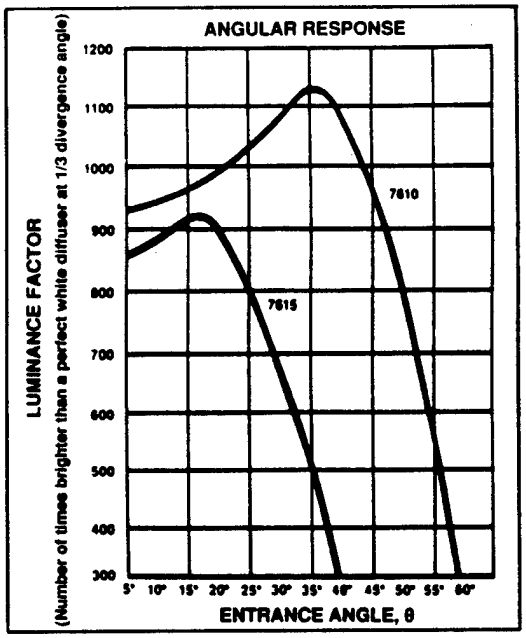

Figure 8. Wide tolerance on orientation of 3M #7615 retroreflecting screen.

SECTION 3

EXPERIMENTS AT 515 nm

Power-through-the-bucket measurements were used to simultaneously characterize the reflectivity and fidelity as a function of the following important experimental parameters: pump intensity, seed intensity, distance between the retroreflecting screen and the crystal, and the orientation of the screen with respect to the crystal.

3.1 REFLECTIVITY AND FIDELITY MEASUREMENTS

While the phase-conjugate images of Air Force resolution charts provide an excellent qualitative picture of the relative performance of SPS conjugators seeded with retroreflector arrays as compared to SPS conjugators seeded by perfectly, diffuse scatterers, Strehl ratios are a more convenient technique for systematically parameterizing the phase-conjugate fidelity as a function of the important experimental conditions.

The experimental configuration used for our Strehl ratio parameterizations of the seeded SPS conjugators is shown in Figure 9. A p-polarized argon-ion laser was focused into the a-face of an HRL-grown Co-doped $BaTiO_3$ crystal of dimensions 9.2(c) X 6.4 X 5.9 mm immersed in index-matching fluid and oriented as shown. The laser light first refracted into the crystal, then fanned to a small angle with respect to the c-axis before exiting the c-face of the crystal. A retro-reflecting screen (3M #7615) placed in the path of the transmitted light added spatial noise to the beam while at the same time retro-directing each fanned filament back onto itself with excellent pointing accuracy. The retro-directed light seeded the stimulated photorefractive scattering process, lowered its threshold, and made it possible for this crystal (which, without a seed, did not have a large

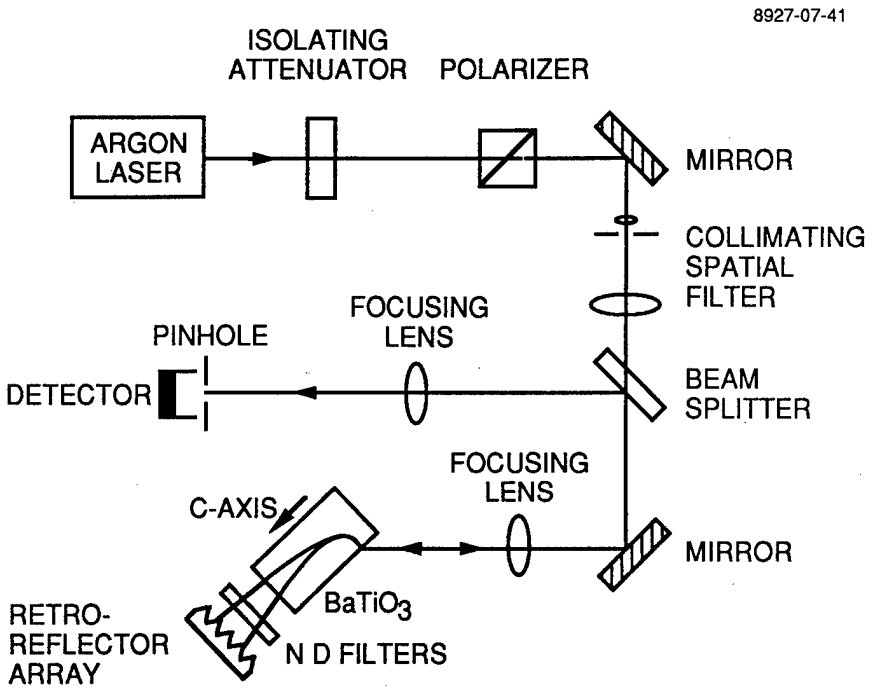

Figure 9. Strehl ratio characterization apparatus.

enough gain-length product to be above threshold) to exhibit the high reflectivity and good fidelity associated with good SPS operation several times above threshold. The reflectivities were calibrated with respect to an ordinary mirror. The fidelity measurements are simply the ratio of the energy through a far-field pinhole of fixed diameter divided by the total energy in the far-field with the pinhole removed.

Two different aberrators were used in these experiments. The initial experiments were performed with a relatively mild aberrator, a glass slide which had been etched in hydrofluoric acid. When sampled with a 1 cm diameter beam, this aberrator resulted in a 1.3 times diffraction-limited beam, as measured at the focus of the 50 cm lens shown in Figure 9. We found that the fidelity of the SPS conjugator was so good that a much more severe aberrator was a better test of its performance. Most of our experiments were performed with a 3.7 times diffraction-limited aberrator.

3.2 PUMP POWER

Figure 10 demonstrates the effect of changing the intensity of the laser beam entering the a-face of the crystal. The reflectivity is a slowly increasing function of intensity while the fidelity is a relatively constant (or possibly slightly decreasing) function of intensity. The pump intensity was adjusted by attenuating it with a rotating polarizing sheet.

The backward SPS reflectivity and the forward SPS, or beam-fanning, both turned off abruptly at threshold power levels which were independent of the intensity incident on the front face of the crystal (i.e. the same power thresholds were observed for several different lens-crystal separations, corresponding to a range of different laser spot sizes on the crystal). These forward and backward SPS pump power thresholds did, however, depend on the degree of spatial aberrations in the laser beam.

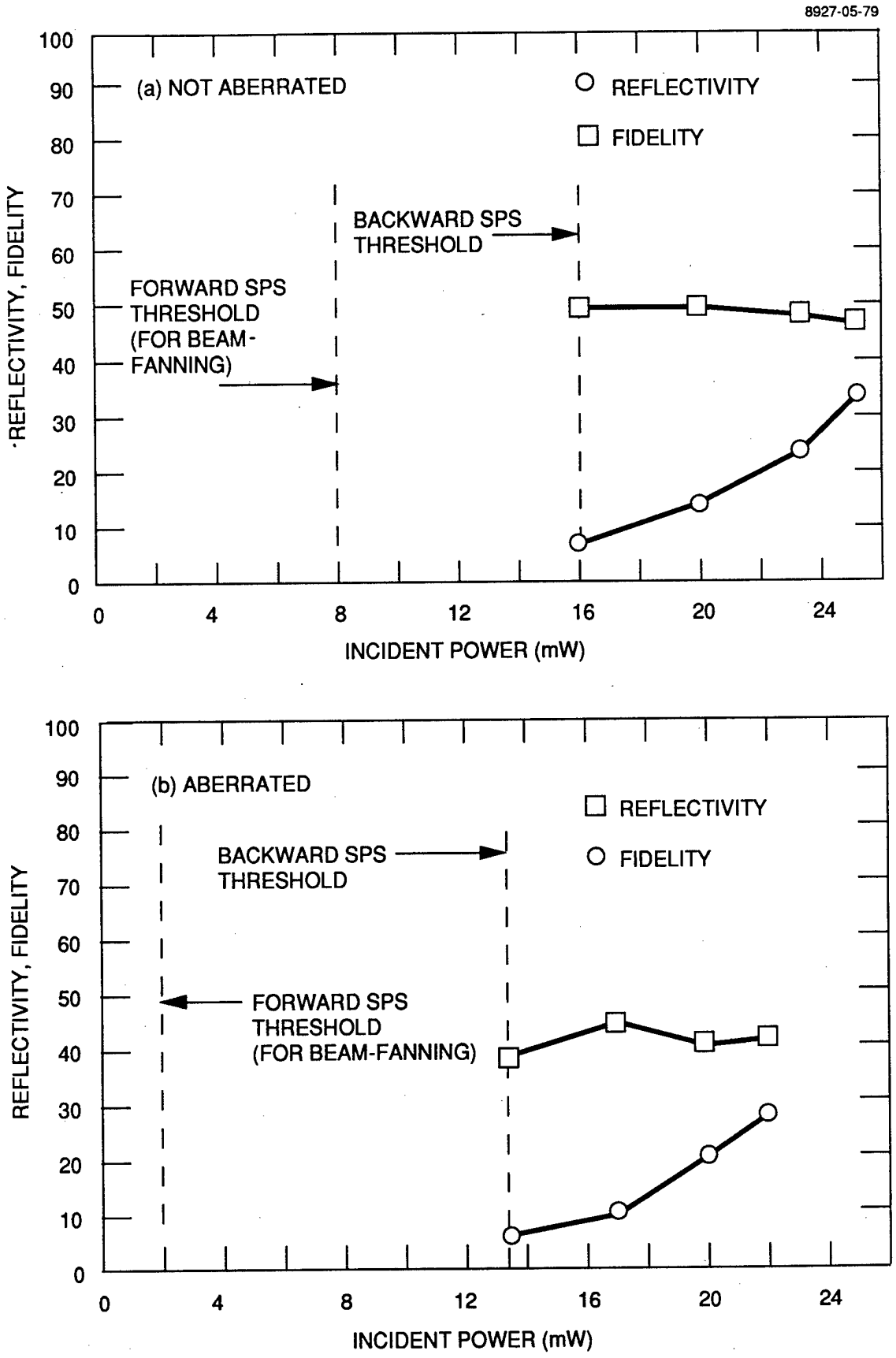

Figure 10. Effect of pump power on reflectivity and fidelity.

Higher forward and backward threshold power levels were measured for the unaberrated beams (16 and 8 mW, respectively, Figure 10a), as compared to when the aberrator was in the system (13.5 and 2.0 mW, respectively, Figure 10b).

3.3 SEED ATTENUATION

A very sharp threshold is observed when measurements of reflectivity are plotted as a function of the seed intensity, Figure 11. For these measurements, neutral density filters were placed between the crystal and the retroreflecting screen.

The reflectivity and fidelity were measured as described above and were plotted as a function of the double-pass transmission of the neutral density filter values. The incident power for these measurements was 52.3 mW. Without any neutral density filters, and with the retroreflector array blocked by a detector (for a phase-conjugate reflectivity of zero), about 5.7 mW was transmitted through the crystal and tank. The reflectivity of the retroreflector array was measured to be 13.7% at 633 nm. Noting from the figure that the threshold occurred for a double-pass neutral density filter transmission of about 5%, we can ascribe to the seed a power threshold of 3.9 μW. In order to estimate the associated threshold intensity, we note that the fanned beam exiting the crystal was typically about 2.5 mm diameter before the onset of SPS (just slightly larger than in the arrangement used for the photos in Figure 4). This corresponds to a threshold intensity of 79 $\mu W\ cm^{-2}$. This threshold intensity should be related to the equivalent dark intensity of the crystal. In a separate experiment with a similarly-colored, but nominally undoped crystal (69D, grown by Sanders and Associates), 300 $\mu W\ cm^{-2}$ was measured to be an upper limit on the equivalent dark intensity of 0.48 μm-period gratings. These two measurements are physically consistent with one another, assuming that the dark conductivities (and associated equivalent dark intensities) of the two different crystals were comparable.

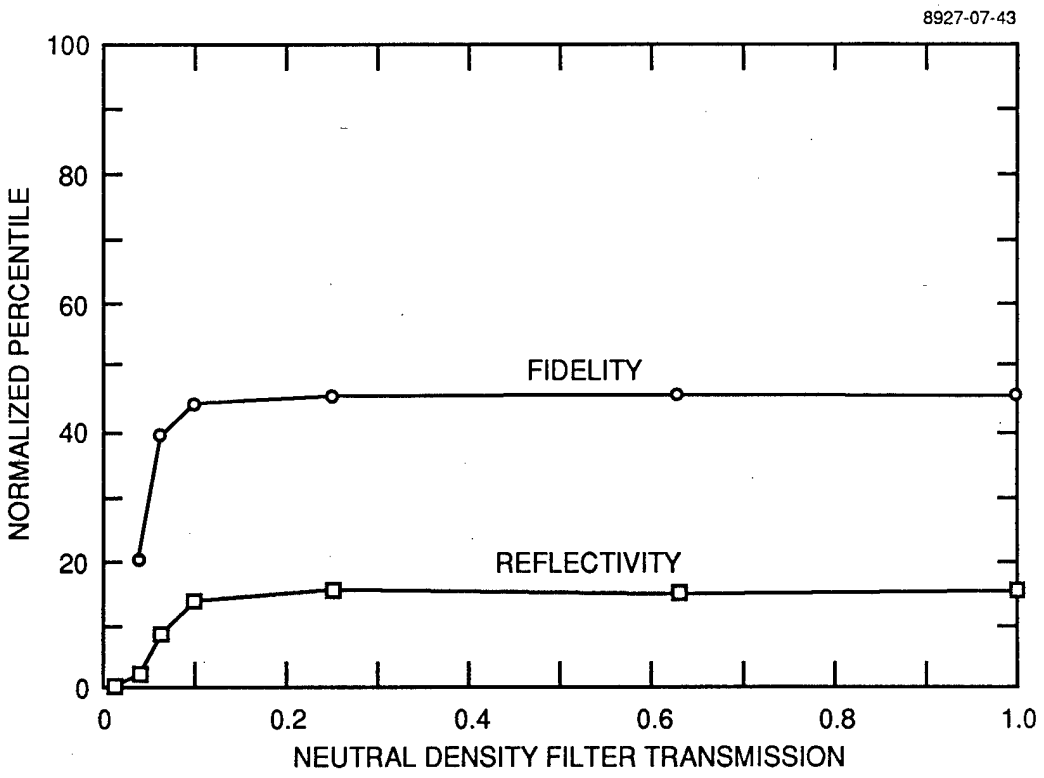

Figure 11. Effect of seed attenuation on reflectivity and fidelity.

For the fidelity measurements just described, we found it very important to make sure that the beam was perfectly collimated as it entered our phase conjugation measurement apparatus. We took special measures to assure that the beam striking the first beam splitter in Figure 9 was very nearly a perfect plane wave. The beam was carefully spatially filtered as before, but special care was taken to assure that no additional phase distortions resulted from the collimating lens just after the spatial filter. In order to obtain the most accurate possible Strehl ratio measurements, we used a shearing interferometer plate to check to see that the laser beam was precisely collimated before entering the lens which focuses the beam into the crystal. Using this diagnostic, we noted that this collimating lens had been severely distorting the beam. Since this lens was not double-passed in our phase conjugation experiment, the phase distortions resulting from this lens were causing the far-field spot size to be many times diffraction-limited. Rotating the lens around the other way improved the uniformity of the laser's phase front so that essentially perfectly straight fringes ($<\lambda/10$) were obtainable across the ~1 cm beam diameter. The result of removing these spatial aberrations in the beam was that the phase-conjugate reflectivity in the absence of the aberrator dropped by a factor of about three. This again emphasizes the important role played by spatial inhomogeneities in optimizing the performance of SPS phase conjugators.

This degradation in reflectivity associated with the improved wavefront flatness was tolerated in exchange for the improved fidelity calibration. The fidelity of an ordinary mirror in the absence of an aberrator was measured and found to be the same as that of the PCM, to within about 4%.

This data demonstrates that the seeded SPS thresholds can be sensitively controlled by adjusting the attenuation between the crystal and the seeding screen. Other possible means for controlling seeded-SPS thresholds include adjustments of the phase of the light between the crystal and the screen, and the incoherent erasure[21,22] method described in Appendix A.

3.4 BEAM INTERACTION LENGTH

The effect of interaction length on phase-conjugate reflectivities and fidelities was determined by measuring these parameters for several different transverse crystal positions, as shown in Figure 12. The reflectivity and fidelity were both found to be largely independent of crystal interaction length for L>~3.5 mm.

The sharp cut-off in phase-conjugate reflectivity with crystal length may result from either or both of two effects. This cut-off may be direct result of a gain-length product threshold for stimulated scattering. Alternatively, it may have more to do with the finite radius of curvature for the forward SPS or beam-fanning; it may be that for crystal lengths less than 3.5 mm, the beam does not bend sharply enough to reach the optimum angle for maximum backward gain.

3.5 CRYSTAL ANGLE (FIELD OF VIEW)

This phase-conjugator was found to have a field of view of at least 35°, as shown in Figure 13.

3.6 DISTANCE BETWEEN LENS AND CRYSTAL

A 50-cm focal length lens was used to focus a slightly converging beam down into the crystal. The distance between the lens and the focal point was about 34 cm. The transverse position of the crystal was adjusted to maximize the interaction length inside the crystal without clipping the beam on the edge

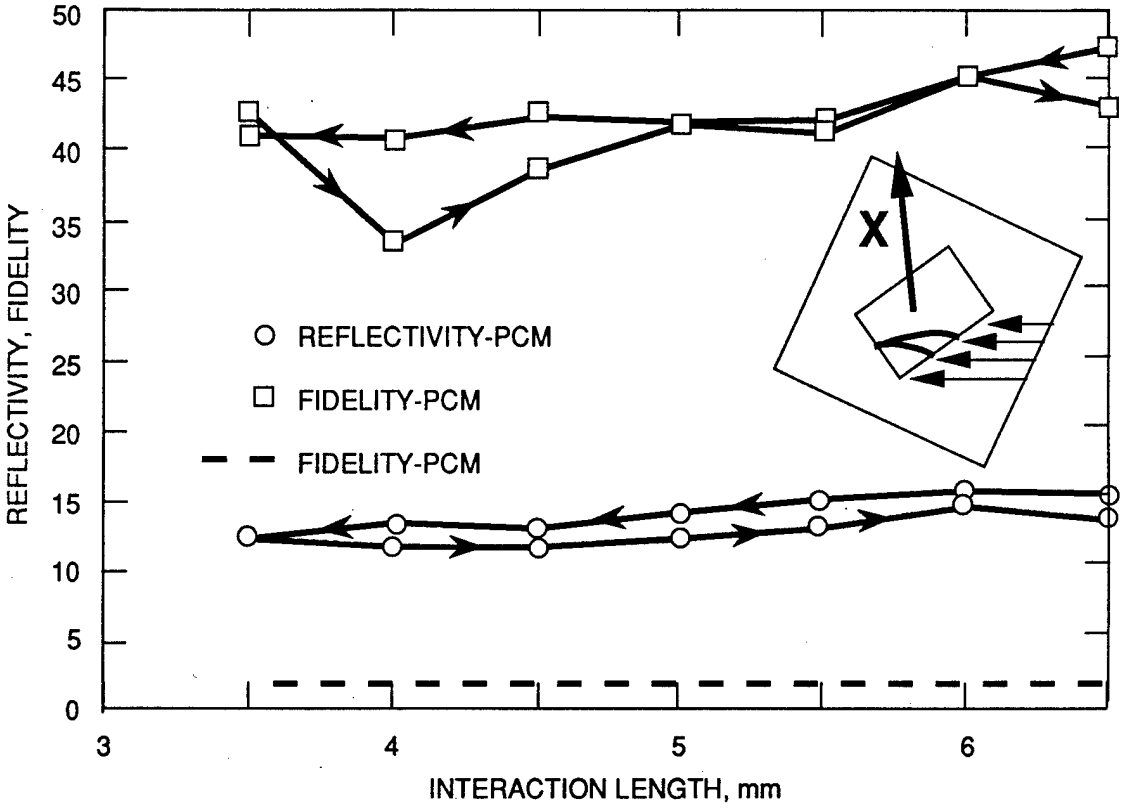

Figure 12. Field-of-view measurement (effect of crystal angle).

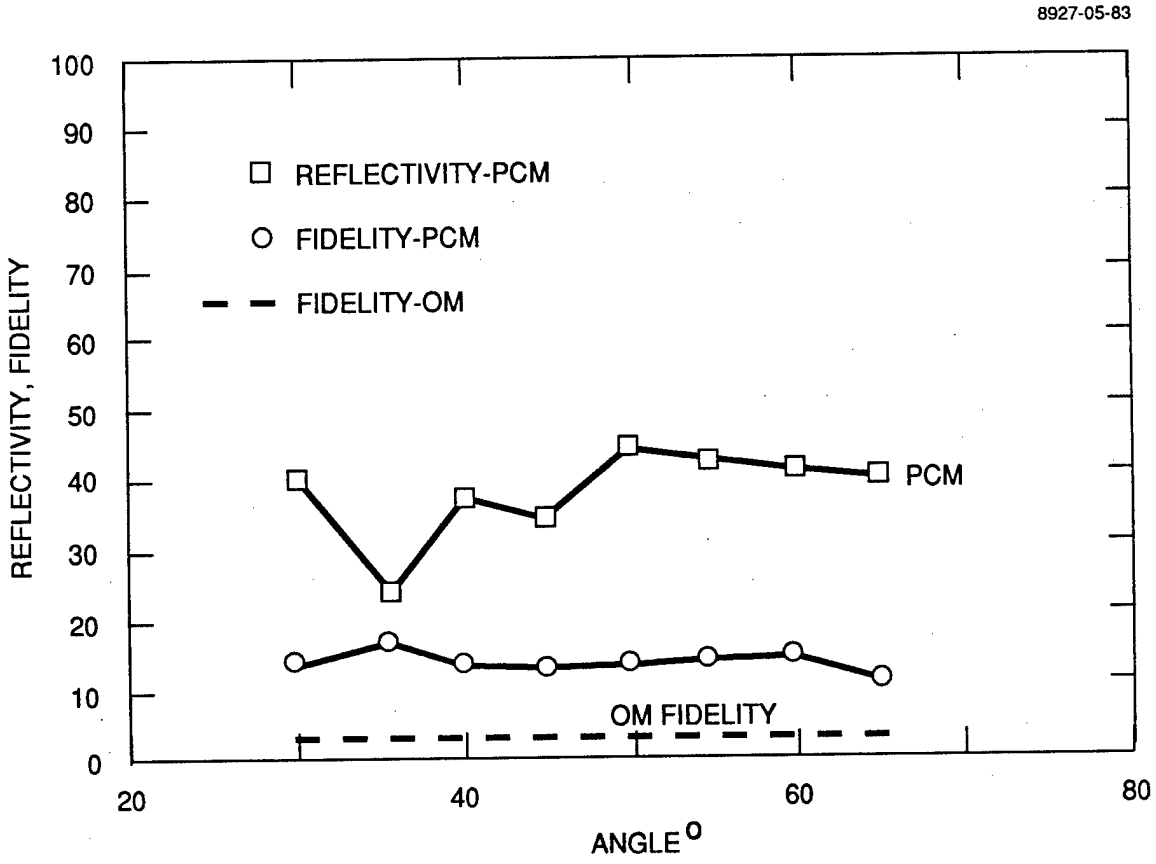

Figure 13. Effect of beam-crystal interaction length.

of the crystal. The crystal was positioned inside a tank of index-matching fluid such that the angle between the c-axis of the crystal and the k-vector of the incident laser beam in air was about 40°. The power incident on the crystal in the absence of any aberrators was about 31.9 mW. Placing a ~3.7-times diffraction-limited aberrator about 5 cm in front of the focusing lens (between the lens and the crystal, such that the beam diameter on the aberrator was ~1 cm), the power incident on the crystal dropped to 27.5 mW.*

The reflectivity as a function of the crystal position realtive to the lens focus is plotted in Figure 14. Positive distances indicate that the crystal is between the focal point and the lens; negative distances indicate that the laser first goes through a focus before entering the crystal.

With the aberrator in place, stable reflectivities of between 30 and 40% were observed on both sides of the focus. Instabilities in the reflectivity were observed when the crystal was positioned at the focus of the laser beam. Without an aberrator, the reflectivity of the crystal positioned at the focus of the laser beam was zero, and no fanning was observed. A finite but unstable reflectivity was observed when the crystal was positioned between about 1 and 3 cm on either side of the focus.

This data highlights the importance of spatial inhomogeneities to stimulated scattering. A cleanly spatial-filtered, unaberrated beam would have little or no spatial inhomogeneities to start with. Placing the crystal at the focal point of such a laser minimizes the spatial inhomogeneities even further, in two ways. First, any residual spatial inhomogeneities (from the focusing lens, for example) would be

* This is the power loss that would be expected from two 7% Fresnel reflections, or from two 4% Fresnel reflections plus an ~8% scattering and/or absorption loss in the aberrator.

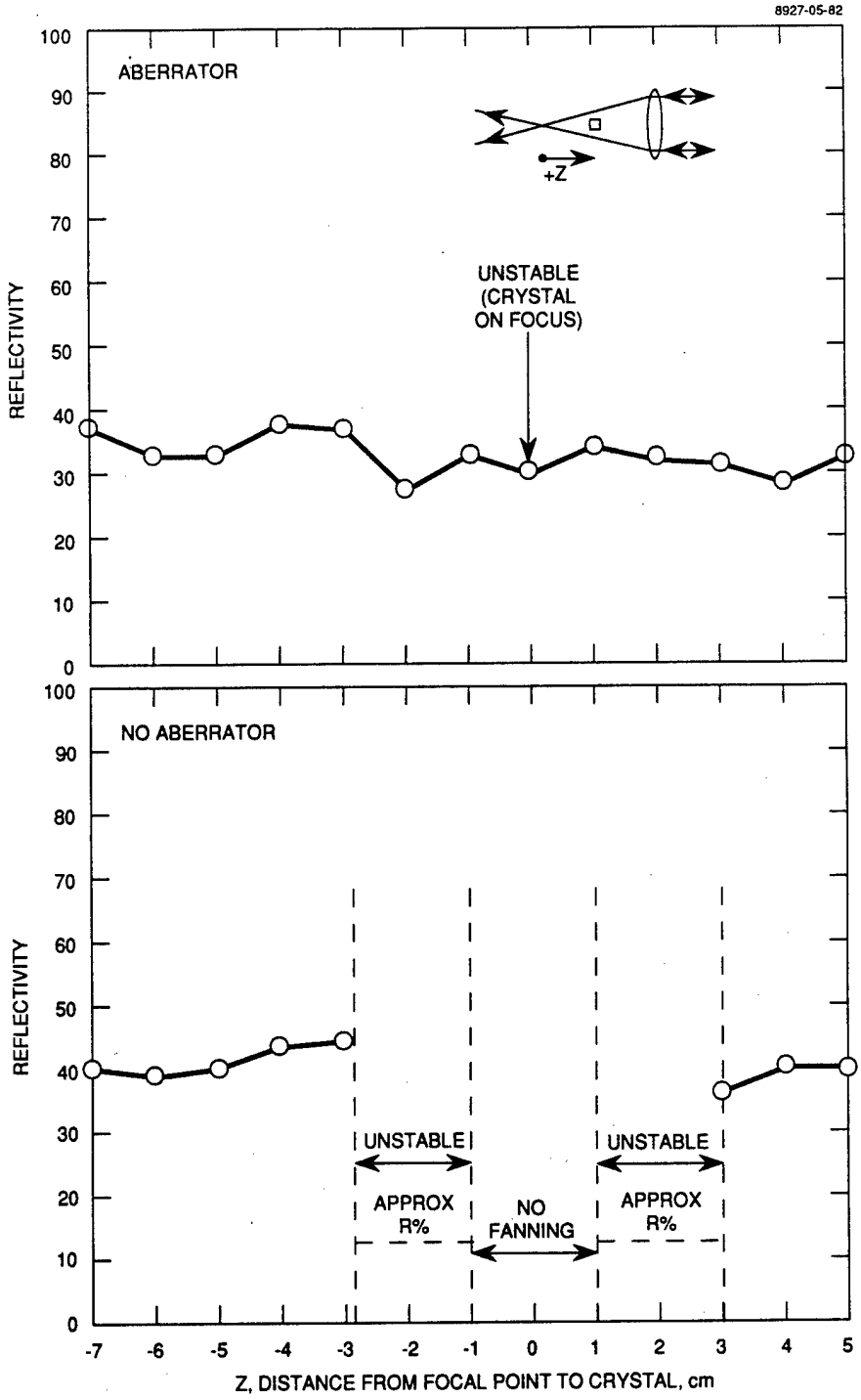

Figure 14. Effect of the distance between the crystal and the lens which focuses the light into the crystal.

thrown out into the wings of the beam in the Fourier transform plane (the focal plane). Secondly, beam inhomogeneities arising from imperfections of the crystal surface are minimized when the beam diameter on the crystal surface becomes small (as near the focal point). For a severely aberrated beam, this second effect would presumably be quite small since the degree of beam inhomogeneities arising from an optically polished crystal surface would be negligible relative to those caused by the aberrating plate. Thus, with the aberrator, the only unstable region of operation is right at the focus, where most of the spatial inhomogeneities arising from the aberrator plate are thrown way out into the wings of the beam and do not mix efficiently inside the crystal.

The above interpretation of the sensitivity of SPS performance on the position of the crystal relative to the laser focus is apparently unrelated to the fact that the intensity of the laser beam is highest at focus. The effect of pump intensity on the SPS reflectivities and fidelities were separately characterized in the series of experiments described in Section 3.2.

When instabilities in the phase-conjugate reflectivity did occur, we found them to be 180° out of phase with the fidelity, as shown in Figure 15.

3.7 POSITION AND ORIENTATION OF SCREEN

The excellent retroreflecting properties of the 3M #7615 screen and the long (several meter) coherence length of our argon-ion laser made the conjugator performance quite insensitive to the position and orientation of the screen.

The insensitivity of the conjugator performance to the separation between the crystal and the screen results from both the long coherence length of the laser and the very high retroreflective accuracy of the #7615 screen, described in

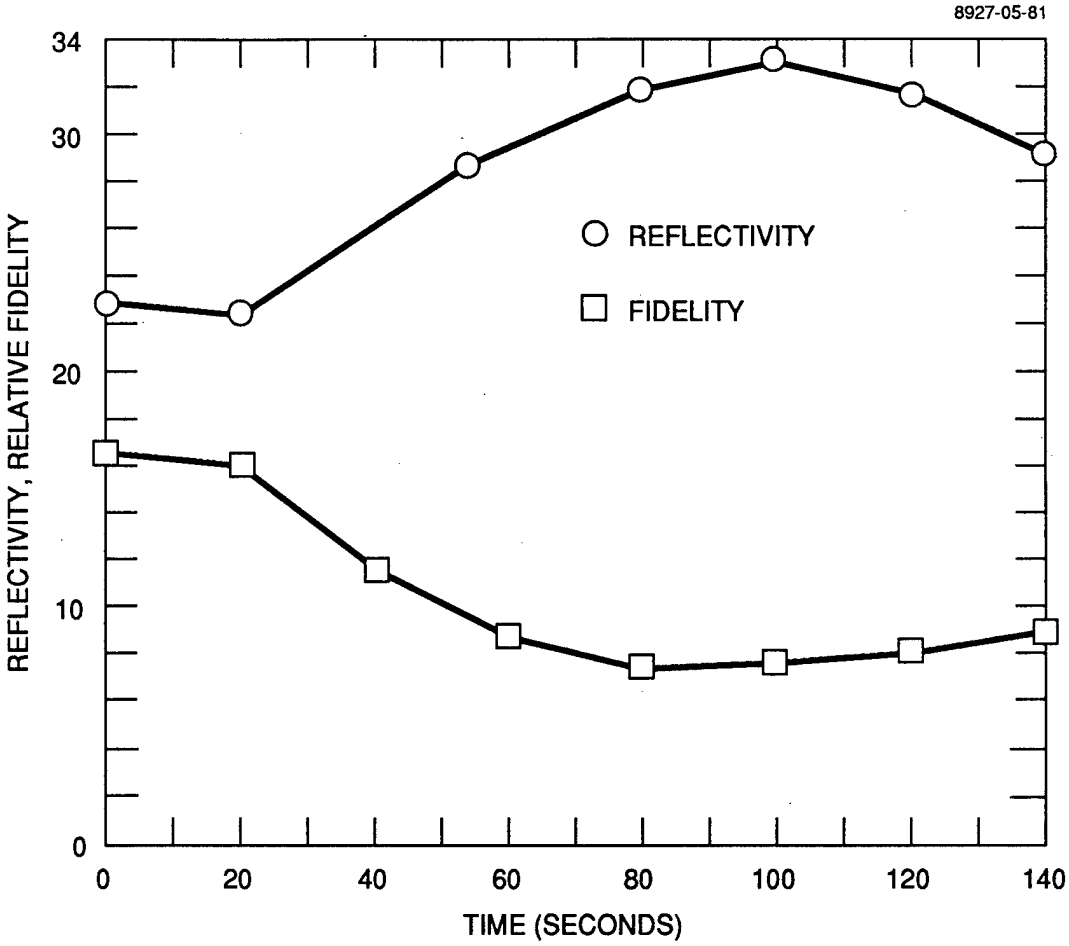

Figure 15. Reflectivity and fidelity oscillations are 180° out-of-phase.

Section 2.2. The laser coherence length was several meters, much longer than the 1-30 cm crystal-screen separations which we tested in our experiment. Our information on the retroreflective accuracy of the screen, from the screen's manufacturer, displayed in Figure 7(b), shows that the array accurately redirects incident rays backwards along the angle of incidence, to within an angle of about 0.5°. This corresponds to a displacement of less than 1 mm for a 10 cm crystal-screen separation. Such beam displacements are on the same order of magnitude as the beam diameter, and can thus be expected to have little or no effect on the seeding accuracy.

The fact that the seeded SPS reflectivity and fidelity were found to be insensitive to the orientation of the retroreflecting screen can be explained by the screen's wide field of view, quantified in Figure 8(b) by the manufacturer's data on reflective efficiency versus angle of incidence, ϕ.

3.8 PERFORMANCE WITHOUT INDEX-MATCHING FLUID

While the most stable, highest reflectivities were obtained when the crystal was immersed in index-matching fluid, seeded SPS phase conjugation was also observed with the crystal in air. The reflectivity was less stable in air because reflections from internal crystal surfaces tended to compete with the seed injected by the retroreflector array. In air, it was difficult to avoid the formation of the internal loop configuration, and the beam trajectory tended to change in time as a result of the competition between the externally seeded SPS and the internal loop. A high-index prism placed in contact with the crystal to spoil the internal reflections effectively eliminated competition from the internal loop under some circumstances, but the stablest performance over the widest range of crystal orientations and positions was achieved with the crystal immersed in index-matching fluid.

3.9 PERFORMANCE WITH BEAM ENTERING C-FACE

Most of our experiments were performed with the laser beam entering an a-face of the crystal, as shown in Figure 4. Seeded SPS operation was, however, achieved with the beam entering the c-face of the crystal. A top-view photograph showing the beam trajectory during seeded SPS phase-conjugation in this geometry is reproduced in Figure 16.

The reflectivity tended to be lower and less stable with the beam entering the c-face than when it entered the a-face. The reason for this improved performance with the beam entering the a-face might be that in this geometry, there is a lot more beam fanning than when the beam enters the c-face of the crystal, as is evident by comparing the two beam trajectory photos, Figures 4 and 16. The beam fanning obviously causes considerable cross-talk between the different spatial modes (or pixels) of the incoming laser beam. It also causes the incoming beam to tend to break up into filaments, as is evident in Figure 4. Both these phenomena (filamentation and cross-talk) play important roles in the selective growth of the phase-conjugate wave at the expense of the non-conjugate noise waves. An excellent description of these effects is given by Zel'dovich et al.[23]

3.10 CONJUGATOR RESPONSE TIME

Our preliminary characterization of the response time of seeded SPS phase conjugation indicates that the conjugator can respond to the removal of the seed in less than a second. A shutter was placed between the crystal and the seed, and the phase-conjugate reflectivity was monitored as a function of time with a power meter and a digital oscilloscope. First, the phase-conjugate reflectivity was allowed to build up to its maximum value with the shutter open. Then, the shutter was closed and the decays of the phase-conjugate reflectivity were measured for several different power levels and for the following two

MC18563-5A 9027-05-38

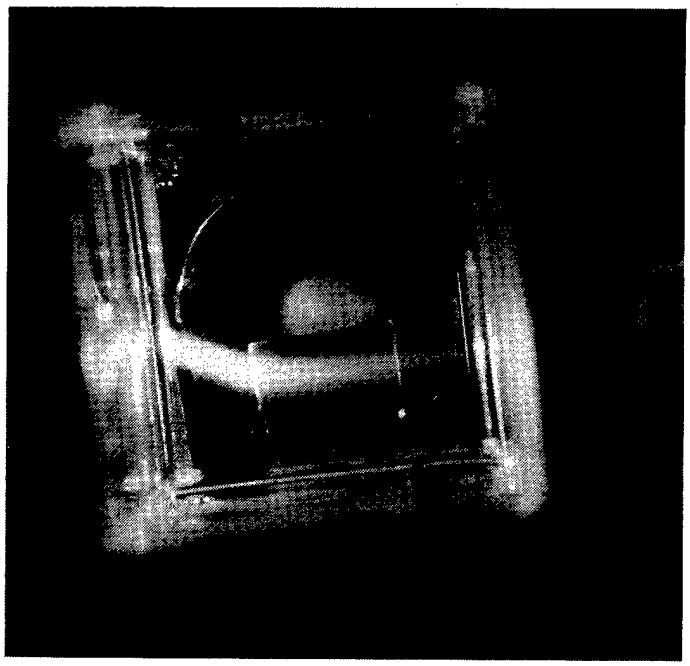

Figure 16. Beam trajectory when beam enters the c-face.

geometries: with the laser beam entering the c-face of the crystal, and with the laser beam entering the a-face of the crystal. The fastest response times (of about 154 ms for 35 mW incident power), seemed to be associated with the geometry in which the beam entered the c-face of the crystal.

The light intensity inside the crystal is known to have a nearly-linear effect on the response rates of these crystals[13]. This may be the main reason why the c-face geometry exhibited faster response rates to the attenuation of the seed than did the a-face geometry. The relative intensities of the seeds in these two cases are evident from comparing the top-view photos of the a-face and c-face geometries shown in Figures 4 and 16 (the high-reflectivity, a-face geometry, and the lower-reflectivity, c-face geometry, respectively). Typical decays of the phase-conjugate reflectivity when the seed is turned off are displayed in Figure 17.

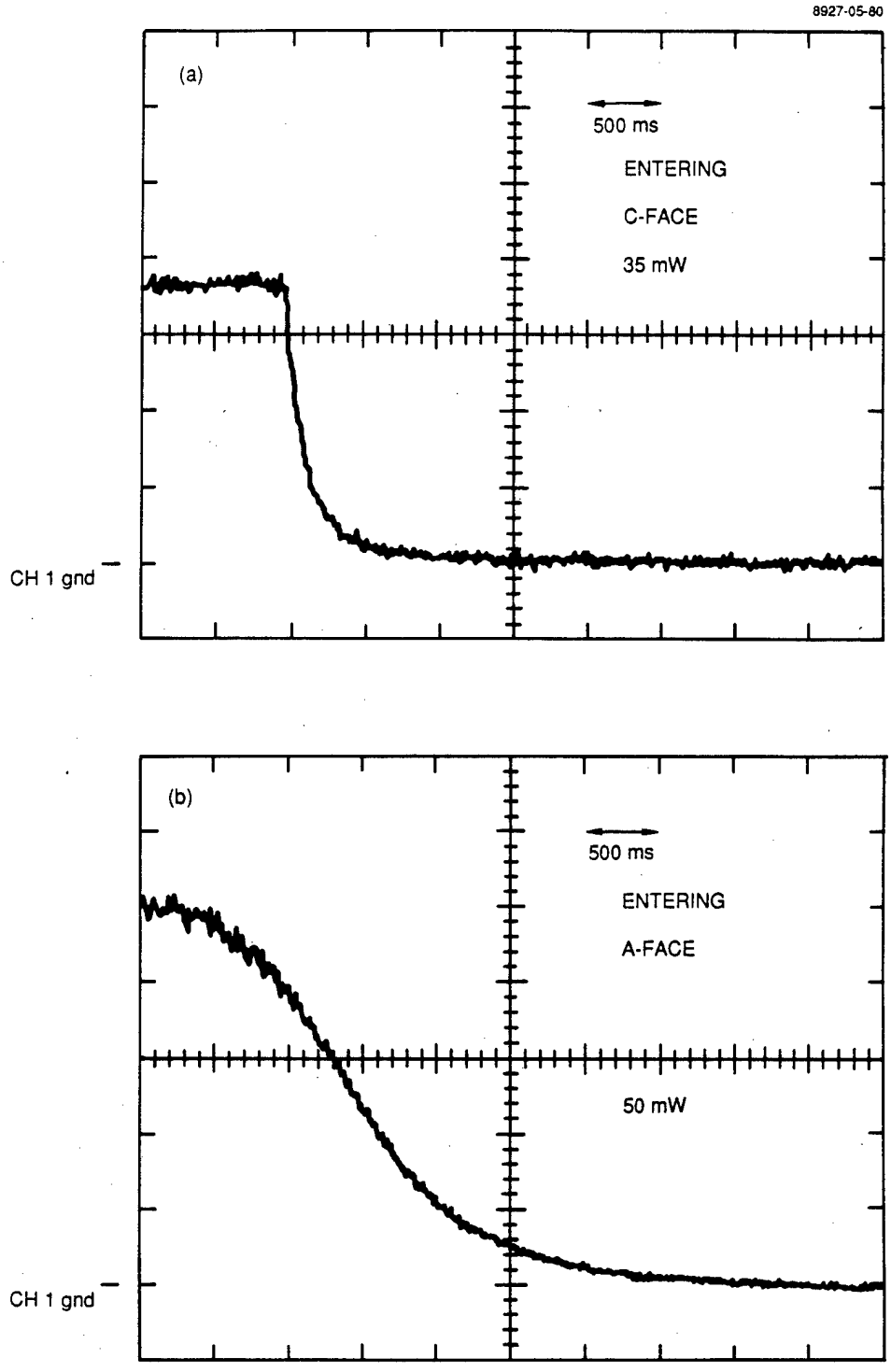

Figure 17. Response time to blocking of seed.

SECTION 4

RED AND INFRA-RED OPERATION

While most of our experiments were performed at 515 nm, we also demonstrated that seeded SPS works at 633 and at 839 nm.

Reflectivities of between 30 and 40% were obtained at 633 nm, using an unfocused 5 mW HeNe laser and the same Co:$BaTiO_3$ crystal which was used for all of the 515 nm experiments described above.

The observation of stable reflectivities at 839 nm was with a crystal grown by Sanders and Associates, boule cut # 120G. Extensive efforts to make the Sanders crystal operate at 839 nm using the internal loop geometry were unsuccessful. The seeded SPS configuration, by contrast, worked easily with this crystal the first time it was tried. The ~5% reflectivity was obtained after about an hour-long exposure with 4.7 mW of optical power. After the seed was blocked, the reflectivity decayed to about 1/e of its initial value in about 54 minutes.

SECTION 5

CONCLUSIONS

A new seeding technique has been developed for phase conjugation via stimulated photorefractive scattering. This new technique makes SPS conjugators practical for a wide range of potential applications at wavelengths ranging from the blue-green into the near infra-red. Several important advantages of the seeded-SPS conjugator over earlier photorefractive phase conjugator geometries were pointed out. The seeded-SPS conjugator has been thoroughly characterised at 515 nm as a function of the following relevant operating parameters: crystal orientation, lens-crystal separation, beam interaction length, incident pump power, attenuation of seed power, crystal-screen separation, and screen orientation. Experiments demonstrating that the seeded-SPS conjugator also works at 633 and 839 nm have been performed.

REFERENCES

1. R.R. Stephens, R.C. Lind, and C.R. Giuliano, "Phase conjugate master oscillator-power amplifier using $BaTiO_3$ and AlGaAs semiconductor diode lasers," Appl. Phys. Lett., 50, 647-649, 1987.

2. M. Minden, R.A. Mullen, and David M. Pepper, "Coherent communication through water using a photorefractive retromodulator/conjugator," submitted to CLEO90.

3. D.M. Pepper, Appl. Phys. Lett., 49, 1001 (1986).

4. D.M. Pepper, Proc. SPIE, 739, 71 (1987).

5. I. McMichael, W.R. Christian, P.H. Beckwith, M. Koshnevisan, P. Yeh, "Phase-conjugate fiber-optic gyros," Paper J8, Topical Meeting on Photorefractive Materials, Effects and Devices, Aussois, France, January 17-19, 1990.

6. J. Feinberg, "Self-pumped, continuous-wave phase conjugator using internal reflection," Opt. Lett. 7, 486-488, 1982.

7. K.R. McDonald and J. Feinberg, J. Opt. Soc. Am. 73, 548, 1983.

8. R.A. Mullen, G.C. Valley, and D.M. Pepper, "Feedback-enhanced stimulated photorefractive scattering," (invited), 19th Winter Colloquium on Quantum Electronics, Snowbird, Utah, January 8-11, 1989.

9. R.A. Mullen, D.J. Vickers, and D.M. Pepper, "Seeded stimulated photorefractive scattering," accepted at the topical meeting on Photorefractive Materials, Effects, and Devices II, Aussois, France, January, 1990.

10. R.A. Mullen, D.J. Vickers, and D.M. Pepper, "Stimulated photorefractive scattering phase conjugators back-seeded with retroreflector arrays," submitted to Conference on Lasers and Electrooptics, Anaheim, CA, 1990

11. R.A. Mullen and D.M. Pepper, in preparation for Optics Letters.

12. R.A. Mullen and D.J. Vickers, in preparation for JOSA B.

13. T.Y. Chang, "Non-linear Optical Studies of Photorefractive Barium Titanate: Parameter Measurements and Phase Conjugation," Ph.D. thesis, University of Southern California, 1986.

14. T.Y. Chang and R.W. Hellwarth, "Optical phase conjugation by backscattering in barium titanate," Opt. Lett., 10, 408-410, 1985.

15. P. Gunter, E. Voit, M.Z. Zha, and J. Albers, "Self-pulsations and optical chaos in self-pumped photorefractive $BaTiO_3$," Opt. Commun., 55, 210-214, 1985.

16. J.F. Lam, "Origin of phase-conjugate waves in self-pumped photorefractive mirrors," Appl. Phys. Lett., 46, 909, 1985.

17. George C. Valley, "Competition between forward- and backward- stimulated photorefractive scattering in $BaTiO_3$," Jour. Opt. Soc. Am., 4, 14-19, 1987.

18. A.V. Mamaev and V.V. Shkunov, "Interaction of counterpropagating waves and phase self-conjugation in a $BaTiO_3$ crystal," Sov. J. Quantum Electron. 19 1199, 1989.

19. J. Feinberg, "Asymmetric self-defocusing of an optical beam from the photorefractive effect," J. Opt. Soc. Am. 72, 46, 1982.

20. R.A. Mullen and D.M. Pepper, "High-brightness diode lasers for blue-green applications," Interim Technical Report, HAC REF G2937, January 1989.

21. Gil Dunning, D.M. Pepper, M.B. Klein, and R.A. Mullen, "Control and optimization of self-pumped phase conjugate reflectivity using incoherent erasure," TuS3, CLEO '89, Baltimore, MD, April 25, 1989.

22. G.J. Dunning, D.M. Pepper, and M.B. Klein, "Control of self-pumped phase-conjugate reflectivity using incoherent erasure," Opt. Lett., 15, 99-101, 1990.

23. B.Ya. Zel'dovich, N.F. Pilipetsky, V.V. Shkunov, Principles of Phase Conjugation, Springer-Verlag, New York, 1985.

APPENDIX A

Control of self-pumped phase-conjugate reflectivity using incoherent erasure

G. J. Dunning, D. M. Pepper, and M. B. Klein

Hughes Research Laboratories, 3011 Malibu Canyon Road, Malibu, California 90265

Received June 19, 1989; accepted October 25, 1989

We use an incoherent erase beam to control optical chaos and to increase the phase-conjugate reflectivity in a self-pumped phase-conjugate mirror. Focused and large-area incoherent illumination was used to modify or eliminate selected gratings in the crystal.

An internal-loop self-pumped phase-conjugate mirror[1] (SP-PCM) is an attractive element for use in optical data processing. Advantages over other classes of PCM's include the inherent simplicity of a single crystal, the avoidance of external pump beams, and the relaxation of certain alignment requirements. However, in certain regimes the operation of a SP-PCM can become unstable.[2–4] In this Letter, we investigate the use of an auxiliary incoherent erase beam to modify and hence control the photorefractive gratings produced in a $BaTiO_3$ crystal during SP-PCM operation. We observe that this technique not only can stabilize the conjugate output but can also increase the phase-conjugate reflectivity.

Use of an auxiliary incoherent erase beam in photorefractive crystals has been used to study the location of photorefractive gratings[5–7] and photoconductivity effects.[8] Devices have also been constructed using an incoherent erase beam, such as incoherent-to-coherent image converters,[9,10] optical bistable devices,[11] and threshold detectors.[12] In our present experiments we use an incoherent erase beam to control the physical location and the temporal characteristics of the gratings in a SP-PCM. Our investigation differs from that of Ref. 5, where an erase beam gated in time and raster scanned in space was used to study photorefractive gratings in the non-steady-state regime. In our research a cw erase beam was employed to study both the steady-state spatial characteristics of the gratings and the time-dependent conjugate reflectivity.

Illumination of the crystal with an incoherent erase beam, i.e., a beam whose phase and frequency are uncorrelated with respect to the input signal beam, locally reduces the modulation depth of the space-charge gratings, thereby reducing the nonlinear coupling gain. Since self-pumping is essentially a stimulated scattering process that starts from noise and exhibits an exponential growth, it has a threshold at a well-defined value of the gain–length product.[1] This condition corresponds to an intensity threshold, if the coupling coefficient varies as $\gamma_0/(1 + I_b/I)$, where I_b is an intensity corresponding to the background conductivity. The threshold value can be controlled, in theory, by illuminating the crystal to change the background conductivity, represented by I_b. The intensity I_b can be written as $I_b = I_d + I_e$, where I_d corresponds to the dark conductivity and I_e corresponds to the erase intensity. By illuminating the crystal with an erase beam, the effective coupling constant will be depressed in the illuminated regions so that those areas will be less likely to contribute to the self-pumped phase-conjugate wave. Alternatively, one can view the erase beam as locally modifying the diffraction efficiency of the photorefractive-induced gratings.

Our experiments were designed so that the input beam and the erase beam could be simultaneously monitored using an architecture similar to that in Ref. 5, where the erase beam propagates perpendicular to the signal beam. The signal beam (514.5 nm) typically was tightly focused near the entrance of the crystal and had a diffraction-limited intensity of 540 W/cm^2. The erase beam operated at 488.0 nm and was incident upon the crystal from below. The polarization and wavelength of the erase beam were chosen to ensure that no photorefractive gratings were written by the erase beam alone or by the interference of the erase beam and the signal beam. Video cameras provided simultaneous monitoring of the erase and signal beams. In all our experiments we used single-domain samples of $BaTiO_3$ grown at Hughes Research Laboratories.[13] One crystal was doped with cobalt (BT58), while the second was undoped (BT29).

Two different erase-beam configurations were used in our studies: large-area erasure and focused small-area erasure. For large-area erasure, the beam was expanded to a diameter larger than the crystal dimension (6 mm × 6 mm × 6 mm), thereby producing a uniform intensity distribution over the entire cross section of the crystal. A movable knife edge was placed in the path to define which portion of the crystal was illuminated by the erase beam. For selective erasure a focusing lens (f = 1.5 m) was placed in the beam at a distance of one focal length from the crystal, which nominally produced a flux of 19.6 W/cm^2 incident upon the crystal bottom surface. Horizontal (x axis) and vertical (y axis) displacements of the focused erase beam were independently controlled. Detectors were used to monitor continually the erase-beam and signal-beam power incident upon the crystal. A mirror located above the crystal was used to image the self-pumping interaction region of the crystal onto a video camera, and an interference filter was used to

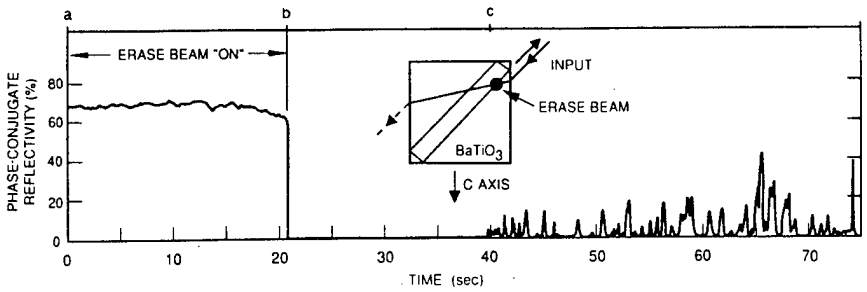

Fig. 1. Temporal behavior of the phase-conjugate return showing elimination of chaos and increased reflectivity in the presence of selective incoherent erasure. The inset shows beam patterns and the location of the erase beam.

reject either the 514.5-nm signal beam or the 488.0-nm erase beam. The signal beam passed through a Faraday rotator and a polarizer to isolate the laser from optical feedback. A U.S. Air Force resolution chart was placed in the path of the input beam for resolution studies, and the beam was then focused into the crystal by a lens (f = 12 cm) to produce the Fourier transform of the mask. The phase-conjugate return was imaged onto a second video camera or monitored by a third detector.

In the first set of experiments, we studied the effect of selective erasure on the temporal stability of the conjugate output of the SP-PCM. Because of the large nonlinearities of $BaTiO_3$, there are regimes of SP-PCM operation where the phase-conjugate output is aperiodic in time.[2,3,14] We determined which geometries and operating fluxes would produce self-pulsations in our crystal. One geometry is shown in the inset of Fig. 1. While operating in this geometry, we illuminated selected areas of the crystal with the focused erase beam. When we illuminated the crystal in the region shown in the inset of Fig. 1, we could eliminate the temporal fluctuations in the conjugate output and, at the same time, produce an increased average cw phase-conjugate reflectivity. The phase-conjugate signal intensity as a function of time is plotted in Fig. 1. The erase beam was present during the time interval between points a and b. As one can see, the output of the SP-PCM was relatively constant during this time. At the time denoted by b, the erase beam was turned off. After an additional ~18 sec, the phase-conjugate signal was reestablished at time c. As can be seen, in the absence of the erase beam the output fluctuated significantly in time and the peak phase-conjugate reflectivity was reduced from the value obtained in the presence of the erase beam.

We postulate the following qualitative explanation for the erase-beam-induced stabilization of the SP-PCM output[4]: When unrestrained (i.e., in the absence of the erase beam), the beams in the crystal will establish themselves in a geometry that produces the highest gain. After the initial loops are formed, pump depletion can reduce the gain in one or more of the beam overlap or interaction regions. This induces a change in the interaction geometry to a new configuation with a higher (undepleted) gain. At this point, the above process repeats, leading to a chaotic output and continously changing beam patterns in the crystal. We and others[14] have observed this instability using a video camera to image the scattered light within the crystal. The observed beam patterns changed in intensity and location as a function of time in a manner that was correlated with the PCM output intensity variations.

In a second set of experiments, we were able to obtain increased phase-conjugate reflectivity relative to that observed in a stable SP-PCM by illuminating the crystal with a focused erase beam. The largest increase in phase-conjugate reflectivity was obtained by illuminating the crystal in a region near the entrance face. The results of these experiments are shown in Fig. 2, where the phase-conjugate return and erase-beam intensities are shown as a function of time. Initially only the 514.5-nm signal beam was incident upon the crystal, resulting in a phase-conjugate reflectivity with an average value of 30%. After approximately 75 sec into the experiment the erase beam was turned on, resulting in an initial reduction of the phase-conjugate return to zero. After an additional 160 sec, and in the presence of the erase beam, the conjugate reflectivity built up to a value that was approximately two times greater than that obtained in the absence of the erase beam.

In the above two experiments we speculate that the erase beam constrains the SP-PCM to operate in a specific interaction geometry that does not allow the formation of additional loops; thus a more stable output results. In addition, the erasure of undesirable competing and/or parasitic gratings[15] results in an increased reflectivity.

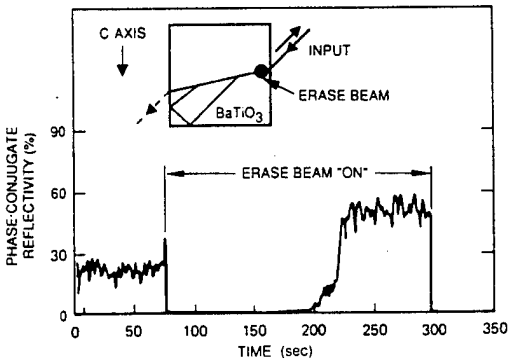

Fig. 2. Enhancement of the phase-conjugate signal beam using selective erasure in an internally self-pumped conjugator. The inset gives the beam pattern in the self-pumped conjugator showing internal loops.

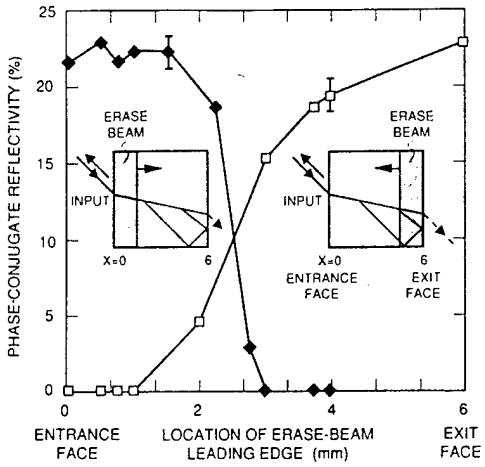

Fig. 3. Plot of phase-conjugate reflectivity versus the area of the crystal illuminated by an incoherent erase beam. The data show the effects of illuminating increasing crystal areas starting from the exit face (open squares) and the entrance face (solid diamonds). The insets are diagrams showing illumination regions of the erase beam (shaded areas).

In a third set of experiments, we measured the reflectivity and fidelity of the phase-conjugate return from a steady-state SP-PCM in the presence of large-area erasure. A knife edge was moved into or out of the erase-beam path to control the extent of the erase beam starting from the entrance or exit face in the crystal. The input signal was a U.S. Air Force resolution chart. Simplified diagrams of the cross section of the experiment are shown in the insets of Fig. 3. The input beam was incident at an external angle of 45° with respect to the surface normal and fanned in the direction of the c axis, forming a typical two-interaction-region pattern within the crystal. The erase-beam area is shown by the shaded area in the figure, with the portion of the crystal illuminated designated by X.

A plot of the phase-conjugate signal reflectivity versus the knife-edge position is shown in Fig. 3. For these experiments, the PCM output was allowed to reach a steady-state value before the erase beam was turned on. The results of these experiments were dependent on the face at which the erasure was introduced. When the erase-beam illumination started from the exit face of the crystal, the phase-conjugate return at each knife-edge setting initially decreased to zero when the erase beam was turned on. After an additional time, which depended on the spatial extent of the illumination, the PCM output would build up to the value plotted in the figure. This type of response suggests that new loops or interaction regions were forming in regions unaffected by the erase beam. When the erase-beam illumination started from the entrance face, the phase-conjugate return did not initially go to zero. Within experimental error, the conjugate reflectivity was initially independent of the knife-edge position and then decreased monotonically as the illuminated region extended further from the entrance face. This result indicated that the erase beam did not effect the loop formation until a critical interaction region near the origin of the loop.

In ongoing experiments, we are examining the fidelity of the phase-conjugate return in the presence of the erase beam for the experimental cases discussed above. We initially found that the fidelity of the conjugate beam can be degraded for large-area illumination when the edge of the erase beam is close to the critical region, where the internal loops branch off from the input beam. During this characterization of the conjugate fidelity versus the area of the crystal illuminated by the erase beam, we observed edge enhancement of the phase-conjugate return. Therefore, we could not use the traditional Rayleigh criteria to establish spatial fidelity. Finally, we are currently investigating both two-wave mixing gain and external-loop SP-PCM reflectivity and fidelity in the presence of the various erase-beam configurations described above.

In summary, we have described the use of an incoherent erase beam to control the conjugate output from a SP-PCM. We have used an erase beam to eliminate competing gratings and thereby control optical chaos and increase the phase-conjugate reflectivity. Furthermore, we have found the existence of critical regions within the self-pumped crystal that are highly sensitive to the erase beam.

We thank R. A. Mullen, G. C. Valley, and G. Burdge for helpful discussions, D. Rytz and B. A. Wechsler for supplying the $BaTiO_3$ crystals, and R. V. Harold for technical assistance. D. M. Pepper acknowledges the support of the U.S. Office of Naval Research (contract N00014-87-C-0122).

References

1. J. Feinberg, Opt. Lett. **7,** 486 (1982).
2. P. Gunter, E. Voit, M. Z. Zha, and J. Albers, Opt. Commun. **55,** 210 (1985).
3. D. J. Gauthier, P. Narum, and R. W. Boyd, Phys. Rev. Lett. **58,** 1640 (1987).
4. G. C. Valley and G. J. Dunning, Opt. Lett. **9,** 513 (1984).
5. P. Brody, Appl. Phys. Lett. **53,** 262 (1988).
6. D. M. Pepper, Phys. Rev. Lett. **62,** 2945 (1989).
7. A. K. Powell, P. D. Foote, T. J. Hall, and R. E. Burge, Proc. Soc. Photo-Opt. Instrum. Eng. **864,** 90 (1988).
8. R. W. Eason and N. A. Vainos, J. Mod. Opt. **36,** 491 (1988).
9. A. Kamshilin and M. Petrov, Soc. Tech. Phys. Lett. **6,** 144 (1980).
10. Y. Shi, D. Psaltis, A. Marrakchi, and A. Tanguay, Appl. Opt. **22,** 3665 (1983).
11. S. Kwong, M. Cronin-Golomb, and A. Yariv, Appl. Phys. Lett. **45,** 1016 (1984).
12. M. Klein, G. Dunning, G. Valley, R. Lind, and T. O'Meara, Opt. Lett. **11,** 575 (1986).
13. The crystal parameters are given in detail by D. Rytz, B. A. Wechsler, M. H. Garrett, and C. C. Nelson, "Measurements of photorefractive properties in $BaTiO_3$," presented at the Topical Meeting on Photorefractive Materials, Aussois, France, January 17, 1990.
14. A. Nowak, T. Moore, and R. Fisher, J. Opt. Soc. Am. B **5,** 1864 (1988).
15. The phase-conjugate reflectivity of an external-loop SP-PCM was increased in the presence of reflection grating washout; see, e.g., M. Cronin-Golomb, J. Paslaski, and A. Yariv, Appl. Phys. Lett. **47,** 1131 (1985).

Observation of Diminished Specular Reflectivity from Phase-Conjugate Mirrors

David M. Pepper

Hughes Research Laboratories, 3011 Malibu Canyon Road, Malibu, California 90265

(Received 28 November 1988)

We observe that the *specular* reflectivity from the input face of a $BaTiO_3$ phase-conjugate mirror *decreases by over 600%* relative to the standard Fresnel reflectivity value upon the onset of phase conjugation, or wave-front reversal. Reasonable agreement is obtained using a model involving the destructive interference of the Fresnel-reflected beam with a series of phase-conjugate waves generated internal to the crystal. The basic diminishing effect should be universal and hence observable in other classes of self-pumped and externally pumped phase conjugators.

PACS numbers: 42.65.Hw, 42.65.Ma, 78.20.−e

The field of nonlinear optical phase conjugation[1] has attracted much interest in both applied and fundamental areas of quantum electronics since its inception in the early 1970's. Wave-front reversal has been demonstrated in most states of matter using myriad nonlinear optical mechanisms including stimulated scattering and parametric interactions. Although the wave-front-reversal nature of these interactions has been intensely studied, no study to our knowledge has been undertaken to characterize the *specular* reflection properties of an *isolated* phase-conjugate mirror. Recently, the specular reflection properties of a Fabry-Perot cavity consisting of a dielectric interface and a semi-infinite phase-conjugate mirror have been investigated;[2] the present study, however, if fundamental to a phase-conjugate mirror itself.

In this Letter, we report on the observation of a significant diminishing of the specular reflectivity from the input surface of a phase-conjugate mirror (PCM). In the case of a $BaTiO_3$ PCM, the near-normal specular reflectivity (in air) was observed to decrease from the standard Fresnel value of $\approx 17.8\%$ to $\approx 2.8\%$ upon the onset of the conjugation process. This striking decrease cannot arise simply from an intensity-dependent refractive-index change at the dielectric interface; indeed, this would require that the index decreases from ≈ 2.45 ($BaTiO_3$) to ≈ 1.4. The required nonlinear index would thus have to be orders of magnitude larger than any previously reported, given our operating intensities ($\approx W/cm^2$).

We deduce that the diminishing effect stems from the destructive interference of a beam undergoing Fresnel reflection at the surface with a *previously unreported beam emerging from the PCM*. The latter beam stems from a sequence of successive conjugation interactions internal to the crystal: A "conventional" volume conjugator which leads to a wave-front-reversed replica, followed by a *previously unreported conjugation process that occurs within one beam diameter of the front surface of the PCM*, and which is mediated via a four-wave mixing[1] interaction. These two internal conjugate mirrors can be shown[3] to be locked in phase relative to each other for all incident angles and wave fronts. The beams generated by this pair of conjugate mirrors combine to interfere destructively with the Fresnel-reflected beam —thereby diminishing its intensity—and, in the process, interfere constructively with the conjugate wave —thereby increasing the externally measured phase-conjugate reflectivity of the conjugator as a whole. The magnitude of the effect depends on the specific nonlinear mechanism(s) internal to the medium, and thus may be material, intensity, and geometry (angle, beam size) dependent. The basic diminishing effect should be universal, and hence observable in other classes of self-pumped and externally pumped PCM's.

We first discuss the basic effect, followed by a description of experimental observations that validate the above conjecture (while ruling out other potential mechanisms), and conclude with a comparison of experimental measurements with model calculations. Various experimental diagnostics lend credence to our model, including the spatial, temporal, polarization, angular, and frequency dependence of the interacting beams,[3] as well as selective optical erasure of the various photorefractive-induced gratings within the crystal.

We assume that all the interacting fields are monochromatic at radian frequency ω_q, with the qth field denoted by

$$\mathbf{E}_q(\mathbf{x}) = \mathbf{A}_q(\mathbf{x}) e^{i[\omega_q t - \mathbf{k}_q \cdot \mathbf{x} + \phi_q(\mathbf{x})]}, \tag{1}$$

where $\mathbf{A}_q(\mathbf{x})$ is real, $\mathbf{k}_q$ is the field wave vector, $\mathbf{x}$ is the propagation direction, and $\phi_q(\mathbf{x})$ is a phase factor depicting the wave front of the field. The basic geometry, along with the two conjugate regions, are sketched in Fig. 1.

Given an input beam, $\mathbf{E}_1$, at frequency ω, the field entering the crystal is $\mathbf{E}_2 = t_F \mathbf{E}_1$, where t_F is the amplitude Fresnel transmission coefficient of the air/crystal interface. The volume phase-conjugate region (PCM_1) generates a conjugate replica of $\mathbf{E}_2$, defined as $\mathbf{E}_3$, and is Stokes shifted in general at frequency $\omega - \delta$:

$$\mathbf{E}_3(\mathbf{x}) = t_F^* r_1 \mathbf{A}_1(\mathbf{x}) e^{i[(\omega-\delta)t + \mathbf{k}_1 \cdot \mathbf{x} - \phi_1(\mathbf{x})]}, \tag{2}$$

where r_1 is the complex amplitude reflectivity of PCM_1 which, in our case, is due to self-pumping[4] in $BaTiO_3$. The detailed mechanisms describing PCM_1—including a random overall phase factor associated with the buildup of stimulated scattering processes from statistical noise fluctuations[1]—are of no consequence to realize the di-

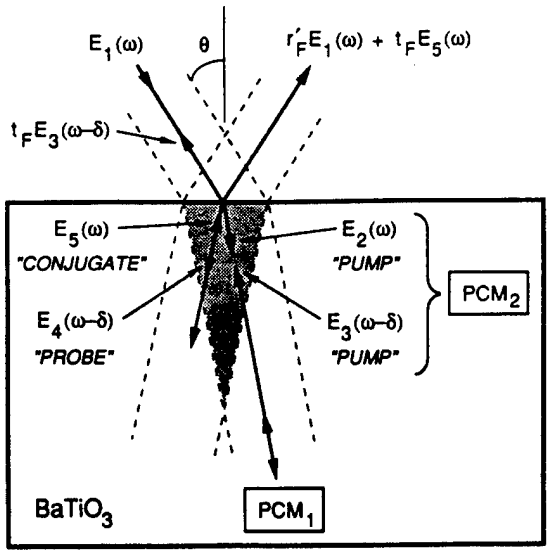

FIG. 1. Schematic diagram of two phased-up conjugation regions that result in a diminished specular reflectivity. PCM_1: Volume conjugator (precise location within crystal not crucial); PCM_2: near-surface conjugator (darker-shaded area).

minishing effect; all that is required is the presence of a conjugate wave within the medium.

The near-surface conjugation region (PCM_2), with amplitude reflectivity r_2 (in magnitude), is mediated by a nearly degenerate four-wave mixing process:[1] The two "pump" beams required for the interaction consist of the incident beam within the crystal ($\mathbf{E}_2$) and its conjugate replica, $\mathbf{E}_3$. These two fields yield a conjugate pair of pump beams, resulting in a phase locking of both PCM's. The "probe" beam incident upon PCM_2, denoted by $\mathbf{E}_4$, is derived from the fraction of the conjugate wave generated by PCM_1 which is internally reflected at the entrance interface into the interaction region of PCM_2, so that $\mathbf{E}_4 = r_F\mathbf{E}_3$, where r_F is the amplitude Fresnel reflection coefficient of the crystal/air interface. As a result of the interaction of the probe wave with PCM_2, a conjugate wave, $\mathbf{E}_5$, at frequency $\omega = \omega + (\omega - \delta) - (\omega - \delta)$ is generated:

$$\mathbf{E}_5(\mathbf{x}) = |t_F r_1 \mathbf{A}_1|^2 t_F r_F^* r_2 \mathbf{A}_1(\mathbf{x}) e^{i[\omega t - \mathbf{k}_1\cdot\mathbf{x} + \phi_1(\mathbf{x})]}. \quad (3)$$

A fraction of this wave, $\mathbf{E}_6 = t_F\mathbf{E}_5$, exits the crystal in the direction of the specularly reflected incident beam, $r_F'\mathbf{E}_1$, where r_F' is the amplitude Fresnel reflection coefficient of the air/crystal interface. These beams, as well as the subsequent reflections, coherently combine, resulting in a total field

$$E_{\text{spec}}(\mathbf{x}) = \{r_F' + |t_F r_1 \mathbf{A}_1|^2 r_2 [t_F^2 r_F^*] + \cdots\}\mathbf{E}_1(\mathbf{x}). \quad (4)$$

Since the phase factor of the product $t_F^2 r_F^*$ differs by π relative to that of r_F', the internally generated wave *destructively* interferes with the specularly reflected incident wave, yielding the diminishing effect. Note that the exiting wave has the same radian frequency (ω) and phase front [$\phi_1(\mathbf{x})$] as the initial specularly reflected wave, $r_F'\mathbf{E}_1$.

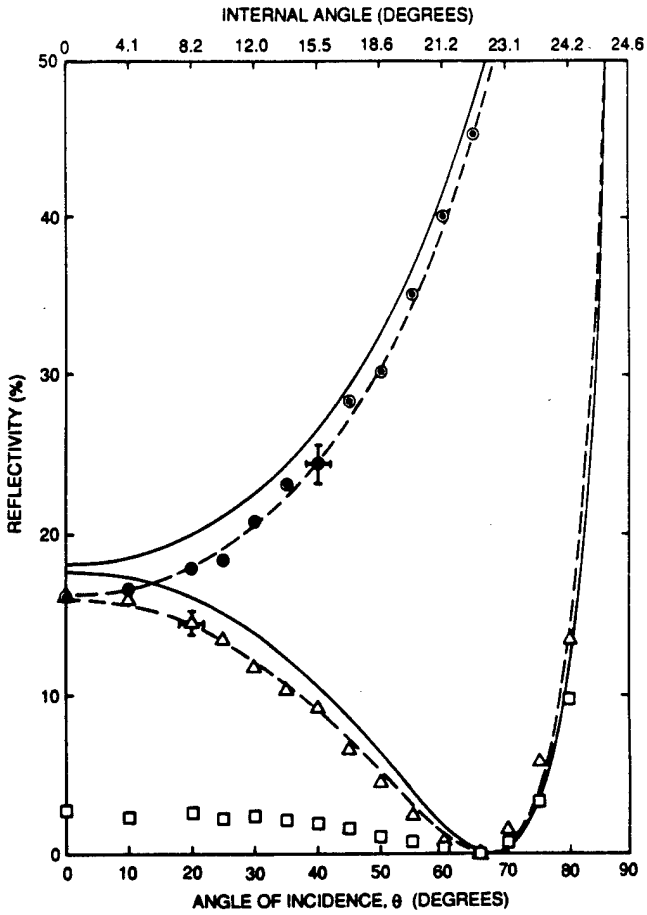

FIG. 2. Specular reflection data for a 45°-cut crystal. *s* polarization (dots): No conjugation and beam fanning occur for this polarization. *p* polarization: Stationary crystal (squares) and angularly dithered crystal (triangles); self-pumped conjugation and fanning occur (do not occur) for the stationary (angularly dithered) crystal. Solid curves: Calculated Fresnel reflectivity for an air/$BaTiO_3$ interface using $n_o = 2.488$ and $n_e = 2.423$, after Ref. 6. [Note: Best fit to our data (dashed curves) was obtained using $n_o = 2.354$ and $n_e = 2.310$; the origin of the small discrepancy is not clear, yet does not affect the basic premise of this paper.]

The experimental apparatus consists of a single-domain crystal of $BaTiO_3$, with a single-longitudinal-mode cw argon-ion laser ($\lambda = 514.5$ nm, $I \approx 440$ mW/cm^2) as the optical source. For this study, both 0°- and 45°-cut crystals[5] were employed. Detectors are used to monitor the specularly reflected beam, conjugate wave, and the residual on-axis beam transmitted (within a $\approx 1°$ field of view) through the crystal.

The specular reflectivity of the 45°-cut sample as a function of the angle of incidence, θ, for both linear polarization states is shown in Fig. 2. For *s* polarization, reasonable agreement is obtained with the standard Fresnel reflection coefficient using the accepted values[6] for the refractive index of $BaTiO_3$. For this polarization

and crystal orientation, self-pumped conjugation does not occur. Similar results were obtained for both crystal cuts.

For p polarization, a dramatic decrease in the specular reflectivity is seen relative to that calculated using the standard Fresnel relations. At near-normal incidence, the reflectivity is 600% smaller than the Fresnel values for the 45°-cut crystal, and is 30% smaller than the Fresnel value for the 0°-cut sample. Since the diminishing effect is seen to occur for all angles of incidence, the effect is *not* due to a fortuitous succession of internal reflections and subsequent interference with the Fresnel-reflected beam. Thus, a well-defined internal beam (in angle and phase) emanates from the conjugator, resulting in the diminishing effect.

When the crystal is angularly dithered about an axis normal to the plane of incidence at a rate (≈ 100 Hz) faster than the characteristic grating buildup time, and through an excursion ($\Delta\theta \approx 0.5°$) in excess of the Bragg acceptance angle, the conjugate wave as well as beam fanning[1] both vanish. Under these conditions, the angular dependence of the specular reflectivity for the p-polarization state is seen to agree reasonably well with the Fresnel-calculated values, as plotted in Fig. 2. Thus, *the diminishing effect has its origins in the nonlinearly induced gratings,* and is not due to an anomalously large nonlinear index or other scattering effect.

The temporal evolution of the specularly reflected beam, conjugate wave, and on-axis crystal throughput is shown in Fig. 3. Since the onset of beam fanning (which temporally precedes the conjugation process) deflects most of the beam off axis, the output of the on-axis detector is seen to decrease in time. On the other hand, the conjugate-wave buildup is temporally correlated with the decrease in the specularly reflected beam. Thus, *the diminishing effect is intimately related to the presence of the conjugate wave within the medium,* and is not related (at least directly) to beam fanning.

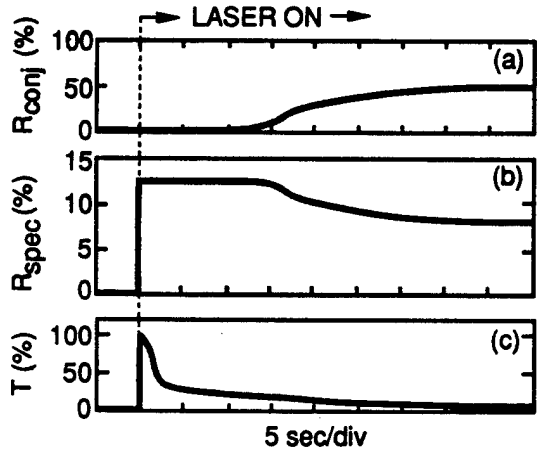

FIG. 3. Observed temporal evolution of (a) the conjugate-wave reflectivity (R_{conj}), (b) the specular reflectivity (R_{spec}), and (c) the normalized on-axis transmission through the crystal (T). For this measurement, a 0°-cut crystal was employed. The conjugate wave buildup to 42.6% reflectivity at ≈ 15 s after laser turn-on is temporally correlated with the diminishing of the specular reflectivity (from 12.7% to 8.7%); beam fanning (resulting in a rapid decrease in transmission) occurs much earlier in time at ≈ 2 s after laser turn-on.

Finally, an incoherent beam with an intensity 10 times that of the probe beam was employed to selectively erase[7] small (≈ 0.2 mm diam) spatial regions of the optically induced gratings in the crystal; illumination was normal to the plane of incidence. In one case, the central portion of the crystal (PCM_1) was illuminated by the erase beam, resulting simultaneously in a restoration of the specularly reflected beam to its Fresnel-calculated value and a complete vanishing of the conjugate beam. When the erase beam illuminated the crystal near the input surface (PCM_2), the specularly reflected beam was again restored to its Fresnel-calculated value; however, most of the conjugate-beam flux persisted (a 40% decrease was observed in the conjugate reflectivity, attributed to optical scattering of the erase beam within the crystal). Hence, we conclude that *two distinct grating regions exist within the crystal:* one which is required for the volume conjugator, and a second near-surface conjugator that contributes to the cancellation of the specular component.

To analyze our system, we employed a generalized treatment of the diminished specular reflectivity model[2] that includes *two* distinct, yet phase-locked PCM's, obtained by summing the terms in Eq. (4). The model predicts a diminished specular (power) reflectivity (R_{spec}), given the Fresnel reflectivity (R_F), and that of the two internal PCM's ($R_{1,2}$):

$$R_{spec} = R_F\{[1-(R_1R_2)^{0.5}]/[1-R_F(R_1R_2)^{0.5}]\}^2, \quad (5)$$

where $R_i = |r_i|^2$. The model also predicts an enhanced overall conjugate reflectivity, R_{conj}:

$$R_{conj} = R_1(1-R_F)^2/[1-R_F(R_1R_2)^{0.5}]^2. \quad (6)$$

Given the externally measured quantities, R_{spec} and R_{conj}, Eqs. (5) and (6) can be solved for the reflectivities of the internal PCM's. From R_1 and typical interaction parameters of the near-surface conjugator—the two-wave gain-length product[8] and the amplitude ratios of the three interacting beams (E_2, E_3, and E_4)—we can calculate[3] its reflectivity, R_2', using a depleted pump analysis.[9] Using the values of R_2' and R_1 in Eq. (5), we arrive at a predicted value of the diminished reflectivity (R_{spec}'), which we compare with our measurements. Results for an internal angle of incidence of 10° are tabulated in Table I. The difference in the magnitude of the diminishing effect for the two crystal cuts arises primarily from their unequal two-wave gain-length products: 0.376 and 1.88, for the 0°- and 45°-cut crystals, respectively. The close quantitative agreement of theory and experiment is fortuitous, given the variation of material parameters and the precise beam overlap geometry.

TABLE I. Calculated and measured specular and conjugate reflectivities for both 0°- and 45°-cut crystals using p-polarized light at an internal (external) angle of 10° ($\approx 24.2°$).

	Specular reflection			Conjugate Reflection		
Crystal cut	Calculated Fresnel refl. R_F (%)	Observed specular refl. R_{spec} (%)	Calculated specular refl. R'_{spec} (%)	Meas. R(PCM) R_{conj} (%)	Calc. $R(PCM_1)$ R_1 (%)	Calc. $R(PCM_2)$ R'_2 (%)
0°	12.7	8.7	9.9	42.6	53.7	3.2
45°	13.2	2.4	2.1	61.4	68.4	59.3

Nonetheless, the observed diminishing effect for the two crystal cuts, coupled with the series of parameter studies, give us confidence that the physical mechanism is well characterized.

In conclusion, we have observed a significant diminishing of the specular reflectivity from self-pumped phase-conjugate mirrors. We have since observed similar diminishing effects in self-pumped conjugators using the "external loop" configuration[10] in $BaTiO_3$ and in $KNbO_3$ (Ref. 11), as well as in $BaTiO_3$ using the standard externally pumped four-wave mixing geometry.[1] The basic diminishing effect should be universal and hence observable in other classes of PCM's, including resonantly enhanced nonlinear media such as sodium vapor,[12] and in stimulated Brillouin scattering PCM's, in which case the near-surface conjugate region may be mediated via a Brillouin-enhanced four-wave mixing process.[13] A practical consequence of the diminishing effect is that unless taken into account, one can inadvertently overestimate the internal volume phase-conjugate reflectivity and hence overestimate the nonlinear susceptibility, as well as underestimate the linear refractive index of the medium. The diminishing effect is expected to be most pronounced in materials possessing large linear refractive indices and nonlinear susceptibilities, such as semiconductors and electro-optic oxides.

The author acknowledges fruitful discussions with G. C. Valley, M. B. Klein, Y. Kohanzadeh, and J. Feinberg, and the technical assistance of J. Schmid. Support of this research by Hughes Research Laboratories and by the U.S. Office of Naval Research under Contract No. N00014-87-C-0122 is gratefully acknowledged.

[1]*Optical Phase Conjugation*, edited by R. A. Fisher (Academic, New York, 1983); B. Ya. Zel'dovich, N. F. Pilipetsky, and V. V. Shkunov, *Principles of Phase Conjugation*, Springer Series in Optical Science Vol. 42 (Springer-Verlag, Berlin, 1985); D. M. Pepper, in *Nonlinear Optical Phase Conjugation*, edited by M. L. Stich and M. Bass, The Laser Handbook Vol. 4 (North-Holland, Amsterdam, 1985).

[2]M. Nazarathy, Opt. Comm. **45**, 117 (1983); P. D. Drummond and A. T. Friberg, J. Appl. Phys. **54**, 5618 (1983); I. Lindsay and J. C. Dainty, Opt. Comm. **59**, 405 (1986); I. Lindsay, J. Opt. Soc. Am. B **4**, 1810 (1987); A. T. Friberg and R. Solomaa, J. Opt. Soc. Am. B **5**, 2502 (1988).

[3]D. M. Pepper (to be published).

[4]J. Feinberg, Opt. Lett. **7**, 486 (1982).

[5]Y. Fainman, E. Klancnik, and S. H. Lee, Opt. Eng. **25**, 228 (1986); D. M. Pepper, Appl. Phys. Lett. **49**, 1001 (1986). Both crystals were cut from the same boule and were mechanically and electrically poled. The 45°-cut crystal was derived from a 0°-cut sample via rotation about an a direction [(100)], with $(0\bar{1}\bar{1})$ and $(01\bar{1})$ faces.

[6]S. H. Wemple, M. DiDomenico, and I. Camlibel, J. Phys. Chem. Solids **29**, 1797 (1968).

[7]A. A. Kamshilin and M. P. Petrov, Pis'ma Zh. Tekh. Fiz. **6**, 337 (1980) [Sov. Tech. Phys. Lett. **6**, 144 (1980)]; P. S. Brody, Appl. Phys. Lett. **53**, 262 (1988).

[8]G. C. Valley, J. Opt. Soc. Am. B **4**, 14 (1987); **4**, 934 (1987).

[9]M. Cronin-Golomb, J. O. White, B. Fischer, and A. Yariv, Opt. Lett. **7**, 313 (1982).

[10]M. Cronin-Golomb, B. Fischer, J. O. White, and A. Yariv, IEEE J. Quantum Electron. **20**, 12 (1984).

[11]D. Rytz and Shen De Zhong, Appl. Phys. Lett. (to be published).

[12]Nonlinear laser spectroscopy upon reflection from a sodium cell has been recently performed involving a near-surface interaction region; see, e.g., S. L. Boiteux, P. Simoneau, D. Bloch, and M. Ducloy, J. Phys. B **20**, L149 (1987).

[13]A. M. Scott and K. D. Ridley, IEEE J. Quantum Electron. **25**, 438 (1989).